ROTATING MACHINERY TECHNOLOGY, INC.

PRECISION BEARINGS AND SEALS
TURBOMACHINERY REPAIR
ROTORDYNAMIC ANALYSES

HYDRODYNAMIC JOURNAL BEARINGS - TYPES, CHARACTERISTICS AND APPLICATIONS

John C. Nicholas, Ph.D.

July 1996

HYDRODYNAMIC JOURNAL BEARINGS - TYPES, CHARACTERISTICS AND APPLICATIONS

John C. Nicholas, Ph.D.

ROTATING MACHINERY TECHNOLOGY, INC.
4181 Bolivar Road
Wellsville, NY 14895 USA

John Nicholas received his B.S.A.E. from the University of Pittsburgh (1968) and his Ph.D. from the University of Virginia (1977) in rotor and bearing dynamics. While at Virginia, he authored the tilting pad and pressure dam bearing computer programs that are used by many rotating equipment vendors, users and consultants.

Dr. Nicholas has worked in the turbomachinery industry for the last 18 years in the rotor and bearing dynamics areas, including 5 years at Ingersoll-Rand and 5 years as the supervisor of the rotordynamics group at Dresser-Rand, Steam Turbine Division.

Currently, Dr. Nicholas is part owner, President and Chief Engineer for Rotating Machinery Technology Incorporated, RMT, a company that manufactures high performance tilting pad journal and thrust bearings, sleeve bearings, seals and other replacement parts for the rotating equipment industry for the last 10 years. RMT also specializes in turbomachinery repair, refurbishing and balancing. Finally, RMT performs bearing, seal and rotordynamic analyses.

Dr. Nicholas, a member of ASME, STLE and the Vibration Institute, has authored 30 technical papers concerning tilt pad bearing design and application, pressure dam bearings, rotor-dynamics and support stiffness effects on critical speeds.

FIXED LOBE BEARING STABILITY

Unstable Bearings

Fixed lobe or sleeve bearings have the annoying property of becoming unstable at relatively high speeds and/or light loads. The problem is that sleeve bearings (i.e. all journal bearings excluding tilting pad bearings) support a vertically downward load or force with a displacement that is not directly downward but at some angle with rotation from bottom dead center.

This is illustrated in Figure 1 for a high speed, lightly loaded unstable journal bearing. Note that the bearing eccentricity ratio, ε, is very small and the attitude angle, ψ, approaches 90°. In this manner, a light -Y direction load is supported by a +X displacement. This occurs since the load is so light, the resulting pressure profile becomes very small with very little change from the maximum film to the minimum film locations. Remember that the summation of all vertical components of the hydrodynamic forces times the area must be equal and opposite to the external load, W. Likewise, the sum of all horizontal forces must be zero. This can only occur for attitude angles that approach 90°.

Since a downward load is supported by a horizontal displacement, any downward force perturbation will result in a horizontal displacement which will result in a horizontal force and a vertical displacement, etc. Thus, the bearing produces unstable cross-coupling forces that actually drive the rotor and cause it to vibrate at a frequency that is 50% or less of running speed.

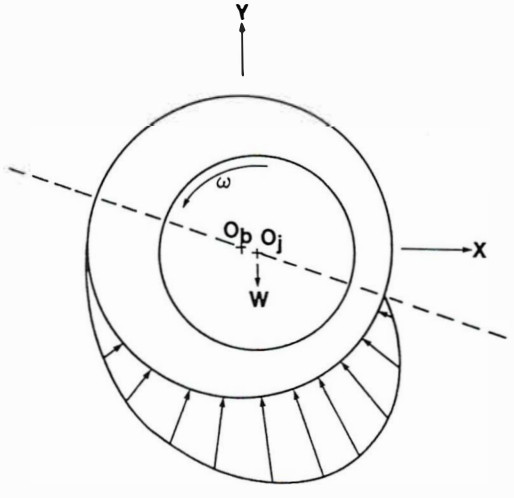

Figure 1 High Speed, Lightly Loaded Unstable Bearing

Stable Bearings

Figure 2 illustrates a relatively low speed, heavily loaded stable journal bearing. Note that the bearing eccentricity ratio, ε, is very large and the attitude angle, ψ, approaches 0°. In this manner, a heavy -Y direction load is supported by a -Y displacement. This occurs since the load is so heavy, the resulting pressure profile becomes very large with very large gradients from the maximum film to the minimum film locations. From a force summation, $\Sigma F_x = 0$ and $\Sigma F_y = W$. This can only occur for attitude angles that approach 0°. Since a downward load is now supported by a vertical displacement, cross-coupling forces are at a minimum and the bearing is stable.

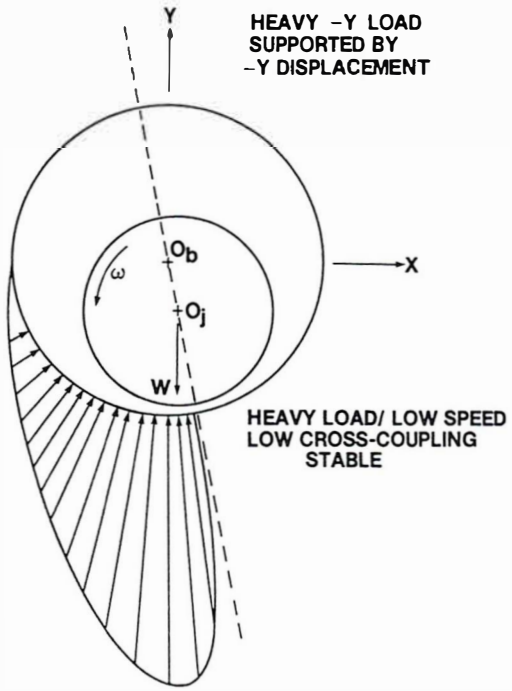

Figure 2 Low Speed, Heavily Loaded Stable Bearing

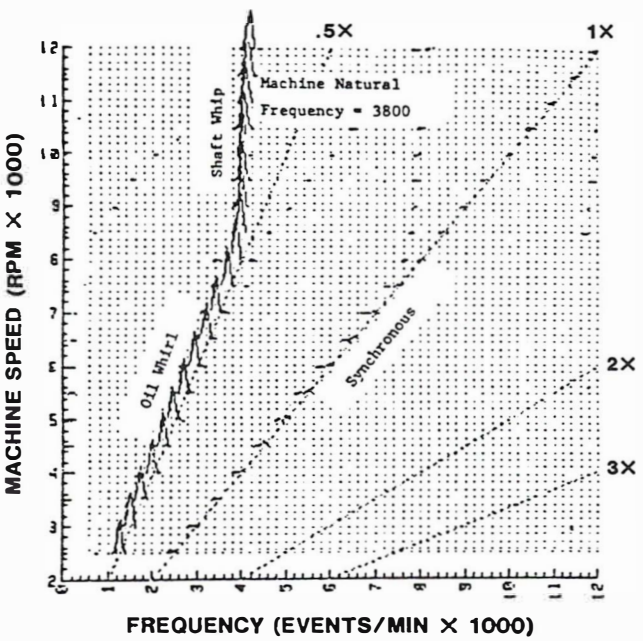

Figure 3 Bearing Induced Shaft Whip and Oil Whirl

Oil Whirl and Shaft Whip

Sleeve journal bearing induced oil whirl and shaft whip are illustrated in Figure 3. The 1x or synchronous vibration line is clearly indicated on the plot. Oil whirl, caused by the destabilizing cross-coupling forces produced by high speed, lightly loaded sleeve bearings, manifests itself as an exact 50% of running speed frequency (shaft vibrates once per every two shaft revolutions). This can be seen in Figure 3 at speeds below about 7,500 RPM (below twice the rotors first critical).

Above 7,500 RPM, the instability frequency locks onto the rotors first fundamental natural frequency, which is at about 3,800 cpm. This re-excitation of the rotor's first natural frequency is sleeve bearing induced shaft whip which shows up as a vibration component that is below 50% of running speed and occurs at speeds that are above twice the rotor's first critical.

Usually bearings are designed not to go unstable until the rotor speed exceeds twice the rotor's first critical speed. Thus, an exact .5x is a rare occurrence and bearing induced instabilities usually show up as shaft whip at frequencies less than 50% of synchronous speed.

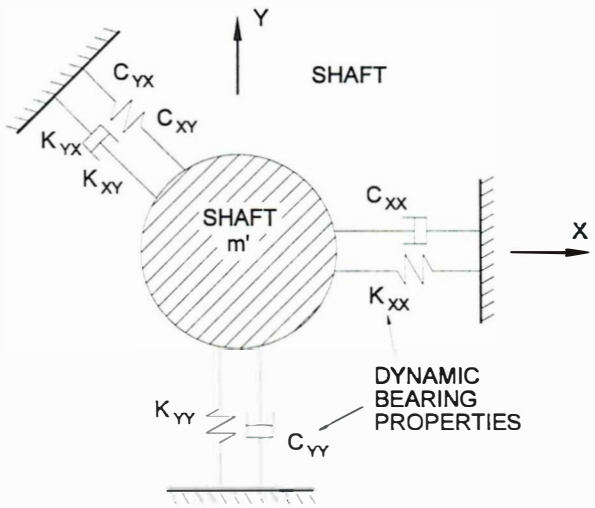

Figure 4 Bearing Instability Threshold Speed Model

Rigid Rotor Instability Threshold Speed

Figure 4 shows an analytical model of a shaft in a bearing. The rotor is represented as a mass, m', and the bearing is represented by 8 stiffness and damping coefficients. As a first step in investigating the stability of the shaft in a journal bearing, the linearized equations of motion in non-dimensional form are derived.

$$\ddot{X} + \frac{W}{m' c_r \omega^2}\left[\bar{C}_{xx}\dot{X} + \bar{C}_{xy}\dot{Y} + \bar{K}_{xx}X + \bar{K}_{xy}Y\right] = 0 \qquad (1)$$

$$\ddot{Y} + \frac{W}{m' c_r \omega^2}\left[\bar{C}_{yx}\dot{X} + \bar{C}_{yy}\dot{Y} + \bar{K}_{yx}X + \bar{K}_{yy}Y\right] = 0 \qquad (2)$$

where

$$\bar{C}_{ij} = \left(\frac{\omega}{c_r W}\right) C_{ij} \quad , \quad \bar{K}_{ij} = \left(\frac{c_r}{W}\right) K_{ij}$$

K_{ij} = bearing stiffness (lb/in)
C_{ij} = bearing damping (lb-s/in)

Assume solutions of the form

$$X = Ae^{i\Omega t} \quad , \quad Y = Be^{i\Omega t} \tag{3}$$

where the real part of the eigenvalue is set equal to zero representing the instability threshold. Setting $\omega = \omega_s$, the instability onset speed, and substituting into equations (1) and (2) yields the following system of equations:

$$\begin{bmatrix} -\left(M'\Omega^2 - \bar{K}_{xx}\right) + i\Omega\bar{C}_{xx} & i\Omega\bar{C}_{xy} + \bar{K}_{xy} \\ i\Omega\bar{C}_{yx} + \bar{K}_{yx} & -\left(M'\Omega^2 - \bar{K}_{yy}\right) + i\Omega\bar{C}_{yy} \end{bmatrix} \begin{Bmatrix} X \\ Y \end{Bmatrix} = \{0\} \tag{4}$$

where

$$M' = \frac{m' c_r \omega_s^2}{W}$$

Equating the real and imaginary parts of the above coefficient matrix to zero yields:

$$\Omega^2 = \left[\frac{\left(M'\Omega^2 - \bar{K}_{xx}\right)\left(M'\Omega^2 - \bar{K}_{yy}\right) - \bar{K}_{xy}\bar{K}_{yx}}{\bar{C}_{xx}\bar{C}_{yy} - \bar{C}_{xy}\bar{C}_{yx}} \right] \tag{5}$$

$$\Phi = M'\Omega^2 = \left[\frac{\bar{K}_{xx}\bar{C}_{yy} + \bar{K}_{yy}\bar{C}_{xx} - \bar{K}_{xy}\bar{C}_{yx} - \bar{K}_{yx}\bar{C}_{xy}}{\bar{C}_{xx} + \bar{C}_{yy}} \right] \tag{6}$$

Define the rigid rotor stability parameter, $\bar{\omega}_s$ as

$$\bar{\omega}_s = \sqrt{\frac{\Phi}{\Omega^2}} = \sqrt{M'} = \omega_s \sqrt{\frac{m' c}{W}} \tag{7}$$

The linear bearing coefficients may be used to determine the non-dimensional instability threshold speed, $\bar{\omega}_s$, from equations (5), (6) and (7). Then, the speed at which the journal becomes unstable may be determined from

$$\omega_s = \bar{\omega}_s \sqrt{\frac{W}{m' c}} \quad \left(s^{-1}\right) \tag{8}$$

$$N_t = \frac{30}{\pi} \bar{\omega}_s \sqrt{\frac{W}{m' c}} \quad \text{(RPM)} \tag{9}$$

An example of the above formulation is shown in Figure 5. This is a plot of the Sommerfeld Number, S, a dimensionless grouping of bearing parameters, as a function of the dimensionless instability threshold speed, $\bar{\omega}_s = \bar{\omega}$, for several different bearings. This plot was obtained by running a bearing program for each bearing type over a speed range to determine the bearings stiffness and damping coefficients. Then, equations (5), (6) and (7) are used to calculate $\bar{\omega}_s$. From Figure 5, at high journal speeds and/or light bearing loads (high Sommerfeld Numbers), $\bar{\omega}_s$ for pressure dam bearings is up to five times higher than $\bar{\omega}_s$ for the 2 axial groove bearing.

The above formulation assumes a rigid shaft. Shaft flexibility effects will lower the threshold speed. For the bearing stability curves shown in Figure 5, as the rotor flexibility increases, $\bar{\omega}_s$ for a pressure dam bearing approaches $\bar{\omega}_s$ for a 2 axial groove bearing. A flexible shaft non-dimensional instability threshold speed parameter can be approximated by

$$\bar{\omega}_{sf} = \bar{\omega}_s \left[1 + \left(\bar{\omega}_s^2 \Omega\right) \cdot \left(\frac{W}{m' c \omega_{cr}^2} \right) \right]^{-\frac{1}{2}} \tag{10}$$

The disadvantage of this approximation is that the rigid bearing critical speed, ω_{cr}, must first be determined from a critical speed computer program. However, it is a relatively simple way to include the approximate effects of shaft flexibility in the bearing stability parameter.

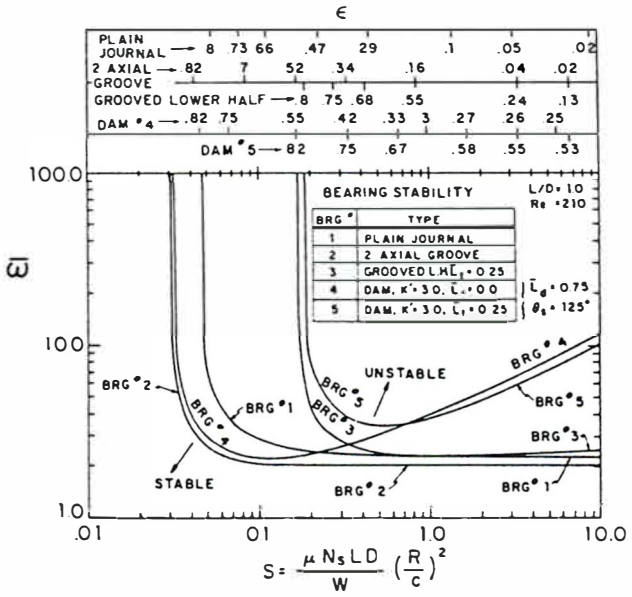

Figure 5 Pressure Dam Bearing Stability Plot

Rigid Rotor Instability Threshold Speed Equations

The journal mass, m′, is defined as

$$m' = \frac{W_j}{g} \tag{11}$$

and equation (9) can be rewritten

$$N_t = \frac{30}{\pi} \bar{\omega}_s \sqrt{\frac{g}{c}} \sqrt{\frac{W}{W_j}} \tag{12}$$

where

N_t	=	rigid rotor instability threshold speed (rpm)
$\bar{\omega}_s$	=	dimensionless threshold speed parameter
W	=	total journal load (lbf)
$W_j = m'g$	=	journal gravity load (lbf)
c	=	radial bearing clearance (in)
g	=	32.174 f/s^2, 386.088 in/s^2
m′	=	journal mass (slug = lbf-s^2/f)

For rotors with additional non-gravity loads such as gear, steam or volute loads, define these non-gravity external loads as

R' = resultant external, non-gravity load (lbf)
R_x = horizontal component of external, non-gravity load (lbf)
R_y = vertical component of external, non-gravity load (lbf)

$$R' = \sqrt{(R_x)^2 + (R_y)^2}$$

For horizontal rotors:

$$W = \sqrt{(R_x)^2 + (R_y - W_j)^2} \qquad (13)$$

W_j = journal gravity load

For vertical rotors:

$$W = \sqrt{(R_x)^2 + (R_y)^2} = R' \qquad (14)$$

W_j = journal gravity load as if the rotor were horizontal

Rigid Rotor Instability Threshold Speed Examples

Calculate the instability threshold speed for a 2 axial groove bearing supporting a 5,000 lbf rotor. The relevant bearing data is given below:

c = .003 in
W_j = 2,500 lbf
D = 4.0 in (bearing diameter)
L = 3.0 in (bearing length)
N = 5,000 rpm (operating speed)

Assuming an approximate viscosity of

$$\mu = 1.11 \times 10^{-6} \text{ lbf} \cdot \text{s} / \text{in}^2$$

Calculate the Sommerfeld Number

$$S = \frac{\mu NLD}{60W}\left(\frac{R}{c}\right)^2 \qquad (15)$$

$$S = \frac{1.11 \times 10^{-6}(5000)(3.0)(4.0)}{60(2500)}\left(\frac{2.0}{.003}\right)^2 = .2$$

From Figure 5, at S = .2, for a 2 axial groove bearing, $\bar{\omega}_s = 2.0$.

Horizontal rotor without external load.

From equation (13), $W = W_j$. From equation (12)

$$N_t = \frac{30}{\pi}\bar{\omega}_s\sqrt{\frac{g}{c}} = \frac{30}{\pi}(2.0)\sqrt{\frac{386.1}{.003}} = 6852 \text{ RPM}$$

Horizontal rotor with a 1,000 lb external load vertically upward.

Thus,

R_x = 0.0
R_y = +1,000 lbf
W_j = 2,500 lbf

Thus, from equation (13)

$$W = \sqrt{R_x^2 + (R_y - W_j)^2} = \sqrt{(1000 - 2500)^2} = 1500 \text{ lbf}$$

and, from equation (12)

$$N_t = \frac{30}{\pi}\bar{\omega}_s\sqrt{\frac{g}{c}}\sqrt{\frac{W}{W_j}} = 6852\sqrt{\frac{1500}{2500}} = 5308 \text{ RPM}$$

Clearly, an upward load that unloads the bearing is destabilizing.

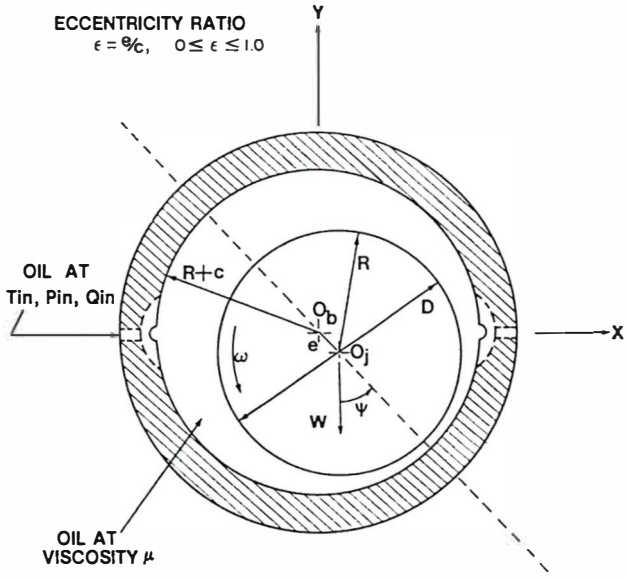

Figure 6 Two Axial Groove Bearing

2 AXIAL GROOVE AND PRESSURE DAM BEARINGS

2 Axial Groove Bearings

Axial groove bearings have a cylindrical bore with typically 2 to 4 axial oil feed grooves. Figure 6 illustrates a 2 axial groove design. These bearings are very popular in relatively low speed equipment. For a given bearing load magnitude and orientation, the stability characteristics of axial groove bearings are primarily controlled by the bearing clearance. Tight clearances produce higher instability thresholds but tight clearance bearings present other problems that make them undesirable. For example, as clearance decreases, the bearing's operating oil temperature increases. Furthermore, babbitt wear during repeated start-ups will increase the bearing's clearance thereby degrading stability. In fact, many bearing induced instabilities in the field are caused by bearing clearances that have increased due to wear from oil contamination, repeated starts or slow-rolling with boundary lubrication.

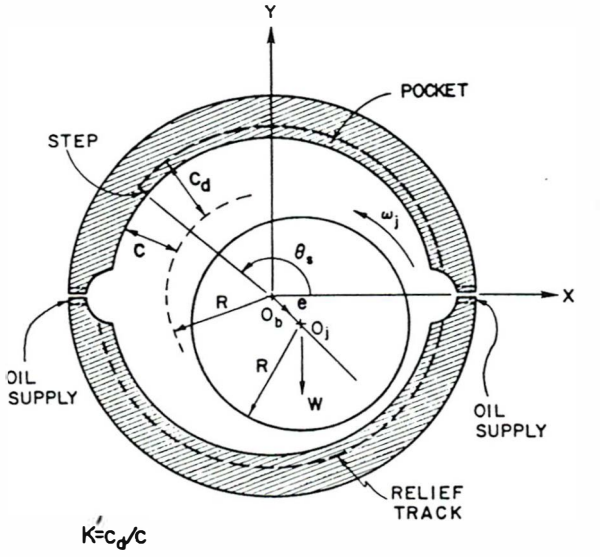

Figure 7 Pressure Dam Bearing - Section View

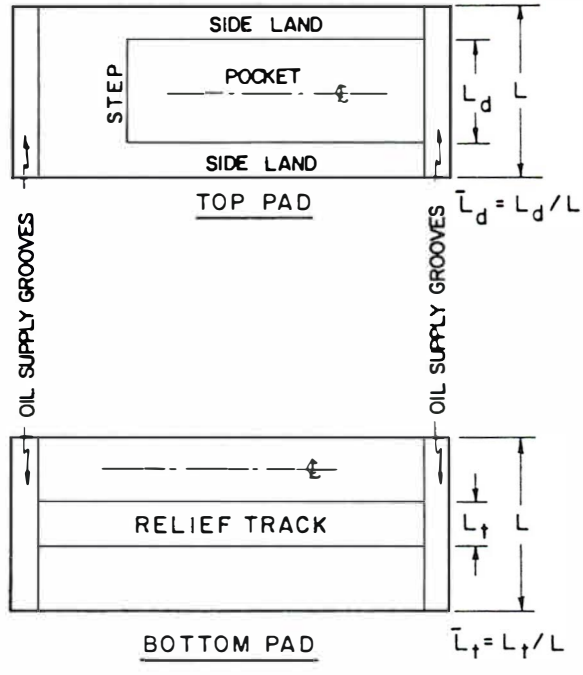

Figure 8 Pressure Dam Bearing - Top and Bottom Pads

Another method of increasing the instability threshold speed of a 2 axial groove bearing is to place a circumferential oil relief track or groove in the bottom half of the bearing (see the bottom pad in Figures 7 and 8). Figure 5 illustrates the stability curves for the grooved lower half bearing (bearing #3) compared to the 2 axial groove bearing (bearing #2). A considerable increase in the infinite stability region is evident for the grooved lower half bearing. That is, the 2 axial groove bearing is theoretically stable at all speeds below a Sommerfeld number of 0.03 while the grooved lower half bearing increases this range to all Sommerfeld numbers below 0.17. Essentially no increase in stability is seen at high Sommerfeld numbers.

The relief track removes some of the bearing's load carrying capacity thereby forcing the bearing to operate at a higher eccentricity ratio. While adding a circumferential groove to the lower half of a 2 axial groove bearing is a popular field fix for a bearing induced instability, care must be taken before this is attempted. First, obviously the fix will only work for bearing operating Sommerfeld numbers below 0.17. Also, this fix should not be attempted for bearing unit loads above L_u = 100 psi.

Pressure Dam Bearings

Because of the limitations described in the preceding paragraph, another fixed-bore anti-whirl bearing design is desirable that is easily manufactured, relatively insensitive to design tolerances, and available for quick retrofits in existing 2 axial groove bearing inserts. The pressure dam bearing falls into this category (Figures 7 and 8, References 1-4). The details of the surface inside the pocket are of secondary importance since the side lands hold the flow and the pressure (4). The hydrodynamic load created by the pocket provides the increased margin of stability for step bearings compared to plain bearings (1-4). Finally, the tolerance on the pocket depth is not as critical as lobe clearance tolerances for multi-lobe bearings (4).

Pressure dam or step journal bearings have long been used to improve the stability of turbomachinery as replacements for plain journal or axial groove bearings. In many cases, these bearings provide a quick and inexpensive fix for machines operating at high speeds near or above the stability threshold. For example, a plain cylindrical axial groove bearing can easily be removed from a machine displaying subsynchronous vibration. Milling a step in the top pad of the proper size and location may be all that is necessary to eliminate the stability problem. This is much less expensive and faster than installing tilting pad bearings that may require a change in the bearing housing.

Most pressure dam bearings have 2 oil supply grooves located in the horizontal plane as shown in Figure 7. For a downward directed load (negative y-direction) corresponding to a portion of the rotor weight, a pocket is cut in the upper half of the bearing with the end of the pocket (the step or dam) located in the second quadrant for counter-clockwise shaft rotation. The pocket has side lands to hold the pressure and flow as shown in Figure 8. A circumferential relief groove or track is sometimes grooved in the bottom half of the bearing as illustrated in Figures 7 and 8. Both of these effects (dam and relief track) combine to increase the operating eccentricity of the bearing compared to a plain cylindrical bearing.

The effect of a stepped pocket on the journal compared to a plain bearing may be easily seen on a bearing eccentricity plot. Figure 9 shows the bearing eccentricity ratio as a function of the Sommerfeld number. The bearing eccentricity ratio, ε, is the amount the journal is offset in the bearing, e (Figure 7) divided by the bearing radical clearance, c. Three curves are plotted on Figure 9. Two different pressure dam bearings with steps located at $\theta_s = 125^\circ$ and 160° are compared to the plain journal bearing curve. All length-to-diameter ratios (L/D) are 1.0.

At high Sommerfeld numbers (light loads and/or high speeds), the plain journal bearing's eccentricity ratio approaches zero and

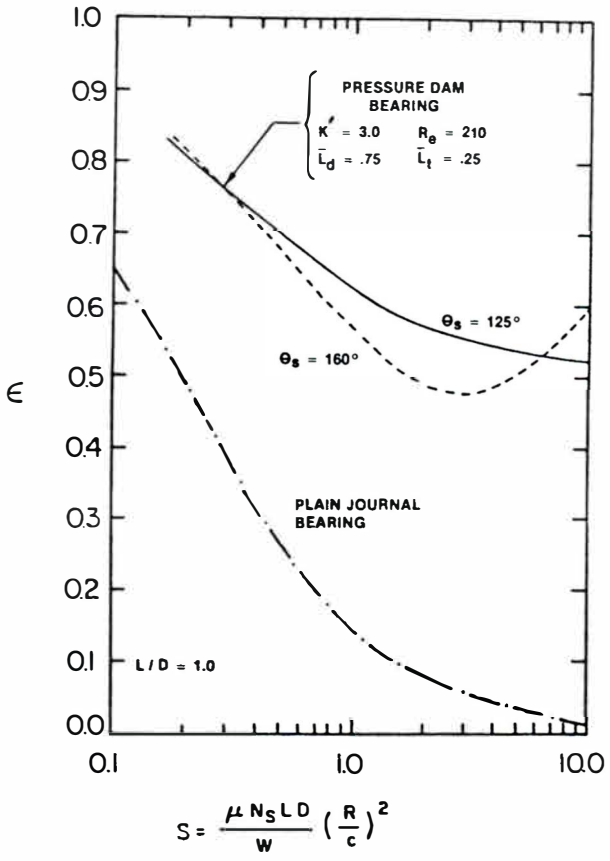

Figure 9 Eccentricity Plots for Pressure Dam and Plain Journal Bearings

the journal runs centered in the bearing. This condition leads to unstable operation. However, the pressure dam bearing eccentricity either approaches some minimum value or increases as the Sommerfeld number increases.

At high speeds and/or light loads, the step creates a loading that maintains a minimum operating eccentricity. That is, as speed is increased, the bearing eccentricity does not approach zero as it would for plain journal bearings. The eccentricity approaches some minimum value or may even increase with increasing speed due to the step loading. Thus, a properly designed step bearing would operate at a moderate eccentricity ratio even at high Sommerfeld numbers. This condition helps to stabilize the pressure dam bearing in the high Sommerfeld number range.

Returning to Figure 5, bearing #4 is a pressure dam bearing with K′ = 3.0 (pocket clearance ratio) and $\bar{L}_t$ = 0.0 (no relief track). For this case, the stability is increased compared to the journal bearing at high Sommerfeld numbers while the region of infinite stability is less. As discussed previously, at high Sommerfeld numbers, the step forces the journal to operate at a moderate eccentricity. From the top of Figure 5, bearing #4 operates at an eccentricity ratio of ε = 0.25 at S = 5.5. This moderate eccentricity provides the favorable stability characteristics at high Sommerfeld numbers for this step journal bearing.

Also from Figure 5, , bearing #5 is a pressure dam bearing with K′ = 3.0 and $\bar{L}_t$ = 0.25 (relief track in bottom pad = 25% of the bearing axial length). In a sense, bearing #5 is a combination of bearing #3 (grooved lower half bearing) and bearing #4 (pressure dam without relief groove) and the resulting stability plot combines the advantages of both designs. Specifically, stability is increased at high Sommerfeld numbers (similar to bearing #4) *and* the region of infinite stability is considerably larger (similar to bearing #3). As before with the grooved lower half bearing, a relief track should *not* be added for bearing unit loads above L_u = 100 psi. Also, a relief track should *always* be added for $L_u \leq 50$ psi.

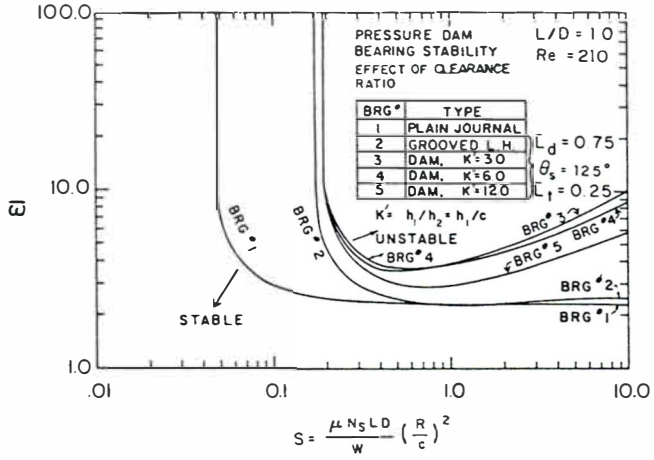

Figure 10 Effect of Clearance Ratio on Pressure Dam Bearing Stability

The effect of varying the clearance ratio, K′, on stability is shown in Figure 10. For a pressure dam bearing, the clearance ratio is defined as (see Figure 7):

$$K' = c_d/c \qquad (16)$$

where c_d = pocket radial clearance, in.
c = bearing radial clearance, in.

The optimum clearance ratio as far as load capacity is concerned is approximately K′ = 3.0 (1-4). Bearing #3 has a clearance ratio of K′ = 3.0 and provides the best stability characteristics. Bearing #4 with K′ = 6.0 is slightly less superior (a 10% decrease at S = 10.0). A 40% decrease in stability is evident for step bearing #5 (K′ = 12.0) when compared to the K′ = 3.0 bearing at S = 10.0. The stability curves for bearing #1 (plain journal) and #2 (grooved lower half) are also included in Figure 10 for comparison.

Figure 11 illustrates the effect of changing the step location on stability. The step is located by the angle, θ_s (Figure 7) measured with rotation, counter-clockwise from the positive horizontal (+X) axis. The optimum step location as far as load capacity is concerned is approximately θ_s = 125° (1-4). This optimum θ_s does provide the optimum stability for $0.2 \leq S \leq 1.7$. However, for S > 1.7, bearing #5 with θ_s = 160° is more stable. In fact, this bearing has two regions of infinite stability ($S \leq 1.7$ and $S \geq 3.4$). As θ_s decreases from 160°, stability decreases at high Sommerfeld numbers.

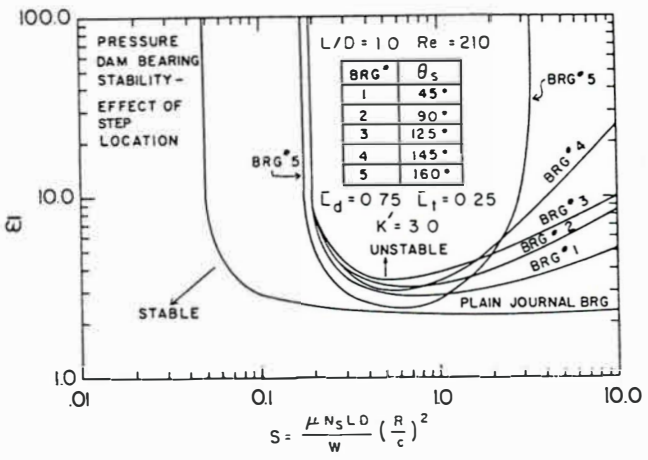

Figure 11 Effect of Step Location on Pressure Dam Bearing Stability

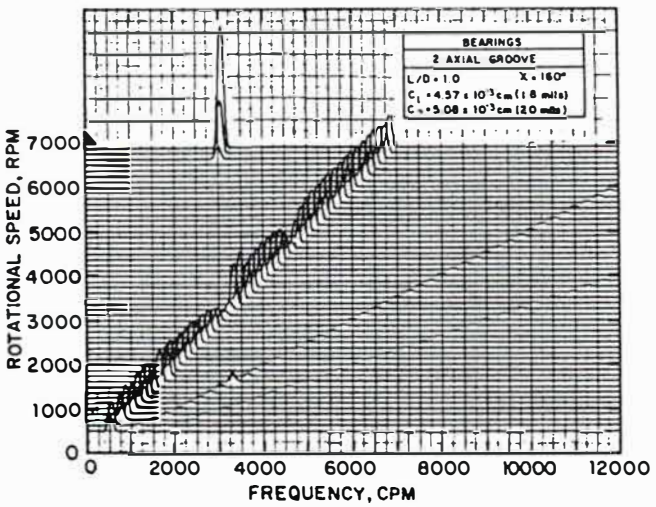

Figure 12 Frequency Spectrum, 2 Axial Groove Bearing

Pressure Dam Bearings - Experimental Results

Figure 12 shows a frequency spectrum for a test rotor with 2 axial groove bearings. A subsynchronous component first appears at about N = 6,600 rpm. Note that Figure 12 indicates that the oil whirl instability manifests itself as a re-excitation of the rotors first fundamental natural frequency of 3,000 cpm.

The theoretically predicted instability onset speed is 6,000 rpm. To obtain this onset speed, the speed-dependent stiffness and damping characteristics are used as input data to a stability computer program that employs a transfer matrix solution. The mass-elastic model of the rotor is also input data to the stability program. A full stability analysis is necessary to accurately predict the threshold speed of a flexible rotor. If equation (9) is used with c = 1.9 mils and $\bar{\omega}_s$ = 2.05, the resulting threshold speed is N_t = 8,823 rpm. Thus, the effect of shaft flexibility is to lower the threshold from the rigid rotor prediction of 8,823 rpm to 6,000 rpm. Note that equation (10) could also be used to approximate the shaft flexibility effects.

The frequency spectrum for a near optimum pressure dam bearing design (K' = 2.1, and 2.4, and θ_s = 145°) is shown in Figure 13. The rotor was run up to maximum speed without a large subsynchronous component appearing. The theoretically predicted instability onset speed is 11,100 rpm.

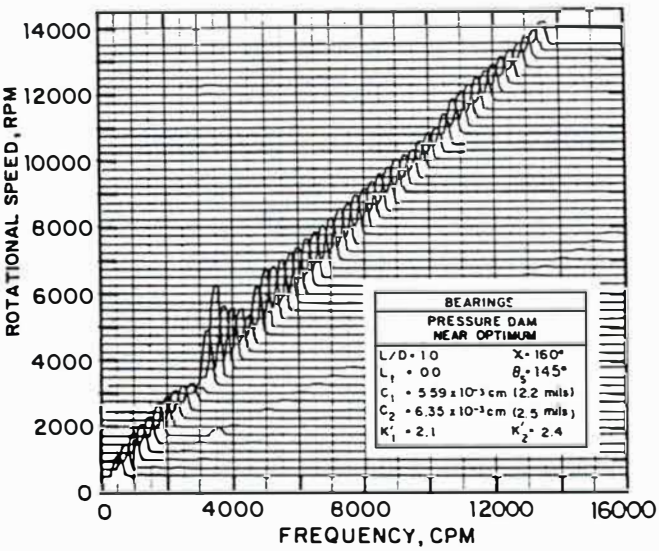

Figure 13 Frequency Spectrum, Near Optimum Pressure Dam Bearing

Pressure Dam Bearing Application - High Speed Gear Box

A large percentage of the rotors used in the rotating equipment industry operate on vendor installed or retrofitted pressure dam bearings. The most common applications are steam turbines and gear boxes. In high speed gear boxes, the gear loading may vary from several thousand pounds at 100% load to only a few hundred pounds at partial load. This large variance in load is often accompanied by a change in load direction. An example is a high speed gear box between the low pressure and high pressure centrifugal compressors in an air compression train for an ammonia plant. In this particular application, step bearings are used in the gear box to ensure stable operation during start-up at partial load

Figure 14 shows the pressure dam bearing design for the high speed pinion. Since the resultant external gear force, W_g, is directed downward, the pressure dam is placed in the top pad. This insures that the bearing's load capacity is at a maximum for 100% load. Note that the 25% and 100% load vectors as well as the minimum film thicknesses for both cases are all located in the bottom pad. Figure 15 shows the pressure dam bearing design for the bull gear. Now, the gear force is directed upward and the pressure dam is placed in the bottom pad. This insures that the bearing's load capacity is at a maximum for 100% load. Note that the 25% and 100% load vectors as well as the minimum film thicknesses for both cases are all located in the top pad.

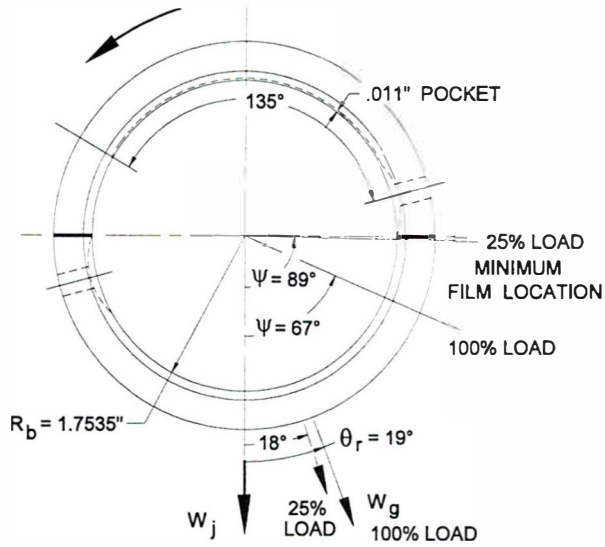

Figure 14 High Speed Gear Box Pressure Dam Pinion Bearing

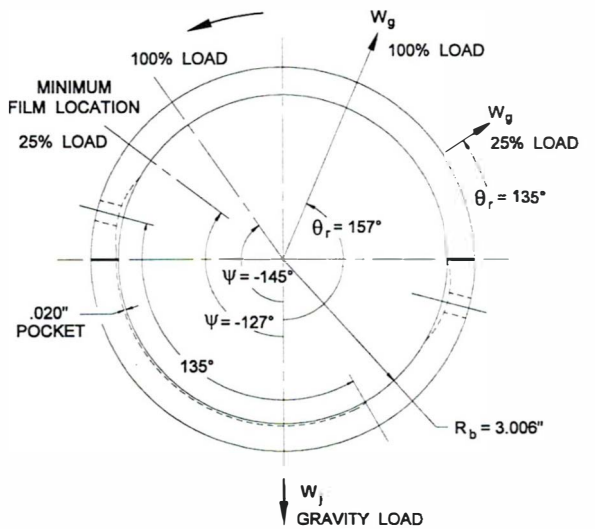

Figure 15 High Speed Gear Box Pressure Dam Bull Gear Bearing

Pressure Dam Bearings - Conclusions

The optimum Sommerfeld number range for designing a pressure dam bearing to increase stability is $S \geq 2.0$. At these high S values, the important design parameters are the clearance ratio, K′ and the step location, θ_s. The optimum clearance ratio in this region is around K′ = 3.0. A slightly larger clearance ratio is recommended to avoid the sudden drop in load capacity for clearance ratios below 3.0. Increasing K′ from 3.0 to 6.0 reduces stability only slightly in the high Sommerfeld number region (only 10% decrease in $\bar{\omega}$ at S = 10.0).

The optimum step location for stability is between θ_s = 125° and 160° depending on the Sommerfeld number. For $S \geq 2.0$, θ_s = 160° is the optimum while for Sommerfeld numbers in the range of $0.2 \leq S \leq 2.0$, 125° is the optimum. A good compromise is θ_s = 140°. A pressure dam bearing designed with these recommended K′ and θ_s values could increase the stability parameter $\bar{\omega}_s$ by a factor of 10 or more over a plain journal bearing at high Sommerfeld numbers. Also, the pressure dam bearing would operate at a moderate eccentricity ratio (between ε = 0.25 and 0.5) even for light loads and/or high speeds.

While the pressure dam or step journal bearings will not solve all rotordynamic instability problems, it remains an extremely effective, low cost anti-whirl bearing. If near optimum clearance ratios and step locations are used, many oil whirl instabilities may be eliminated with pressure dam bearing designs.

ELLIPTICAL AND OFFSET HALF BEARINGS

Another field fix for an unstable sleeve bearing is to elliptize a circular bore by placing a 1.0, 2.0 or even a 3.0 mil shim at top-dead-center between the bearing insert and housing. This has the effect of reducing the vertical bearing clearance and increasing the bearings instability threshold speed.

An elliptical bearing is illustrated in Figure 16. It is essentially a 2 axial groove bearing with a slightly tighter vertical clearance and a more open horizontal clearance. This type of bearing is very popular in Europe and is the standard sleeve bearing design of at least 1 major European compressor manufacturer. It is also used in the United States with at least 1 large domestic motor-generator manufacturer utilizing this design. Elliptizing a pressure dam bearing (5) for improved stability characteristics is also possible (see Table 1).

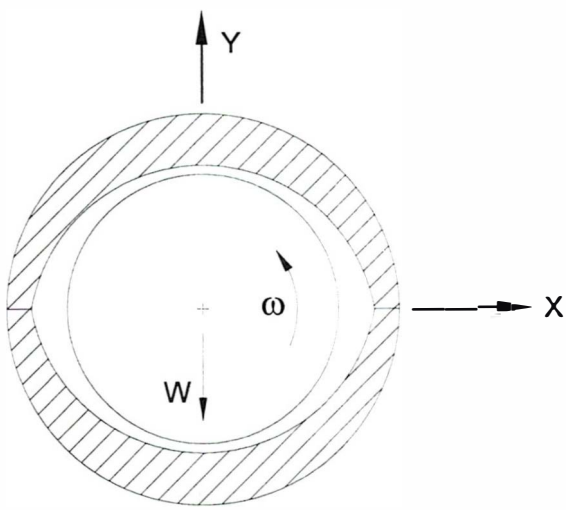

Figure 16 Elliptical Bearing

An integrally geared compressor's low speed pinion bearings induced oil whirl during the partial load start-up. During start-up, a 35% full load condition, the bearing unit loading is L_u = 38 psi. The resultant gear force on the low speed pinion is directed upward similar to Figure 15. The operating speed is 7,766 rpm. Table 1 summarizes the instability threshold speeds calculated with equation (9) for 7 different bearing designs (D = 3.74 in).

Table 1 Integrally Geared Compressor's Low Speed Pinion Bearing Designs

#	Bearing Type	N_t (rpm)	ε	ψ^o
1	2 Axial Groove	8,348	0.42	-34
2	Elliptical	10,660	0.37	-68
3	Elliptical w/ Bottom Half Circumferential Groove	11,587	0.43	-59
4	Elliptical w/ Lower Half Pressure Dam (5)	11,545	0.55	-64
5	Elliptical w/ Lower Half Pressure Dam & Upper Half Groove (5)	15,912	0.67	-83
6	Pressure Dam in Bottom Pad	15,752	0.40	-77
7	Pressure Dam in Bottom Pad w/ Upper Half Groove	19,172	0.66	-109

Remember that these threshold speeds are a rigid shaft approximation and the actual values are lower because of shaft flexibility. Bearing #2 is the as-is design. The final design must be able to tolerate the full load operating condition as well as partial load start-up. Bearings #5 and 7 are eliminated because of poor load capacity while #1 and 2 are eliminated because of instability concerns. Bearing # 6 is the recommended design.

Another method to stabilize a 2 axial groove bearing is to offset the bore usually at the horizontal split. An offset half bearing is shown in Figure 17. This bearing is also very popular in Europe. Offsetting a pressure dam bearing is also possible for improved stability (6).

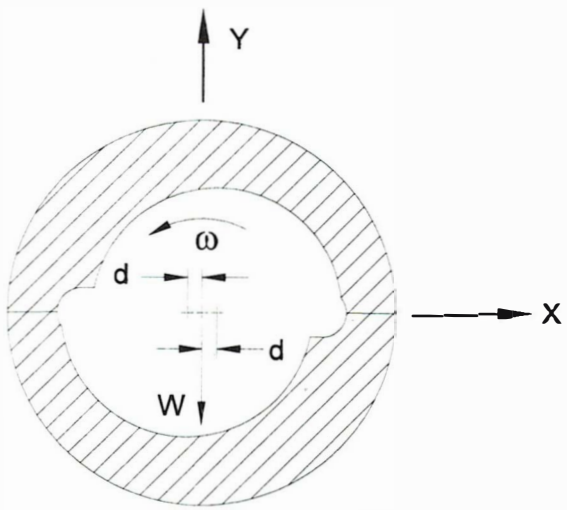

Figure 17 Offset Half Bearing

3 AXIAL GROOVE AND MULTI-POCKET BEARINGS (7 ,8, 9)

3 Axial Groove Bearings (9)

For 3 axial groove bearings (see Figure 18 with h_s = 0.0), clocking the bearing can be very effective in improving stability. The stability curves for a 3 axial groove bearing are shown in Figure 19 for 3 different clockings: clocked 15° against rotation (θ_c = -15°), clocked 15° with rotation (θ_c = +15°) and load directed between oil feed grooves (θ_c = 0°). A much larger region of infinite stability is evident with the -15° clocking. Infinite stability includes all Sommerfeld numbers less than 0.6 for the θ_c = -15° case. This is accomplished by placing the axial oil feed groove in the area of maximum hydrodynamic pressure forcing the bearing to operate at a larger eccentricity ratio for a given Sommerfeld number. This loss in load capacity is illustrated in Figure 20. For example, at S = 0.6, the eccentricity ratio for θ_c = 0° and +15° is ε = 0.5 and 0.54 respectively compared to ε = 0.7 for θ_c = -15° .

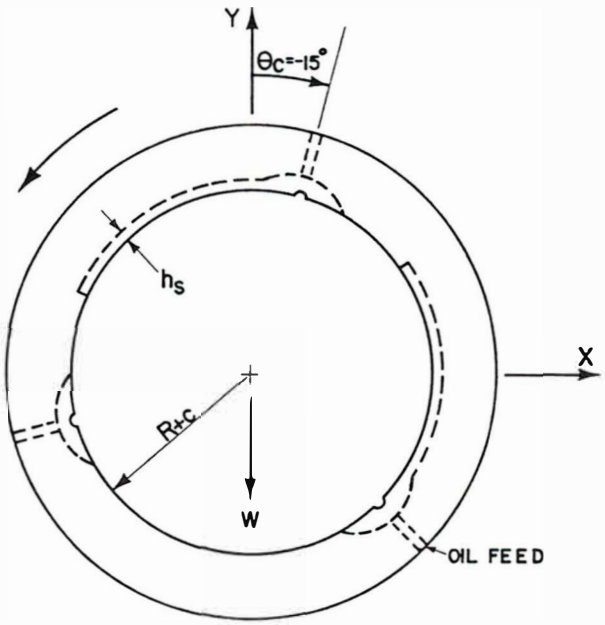

Figure 18 Double Pocket Bearing

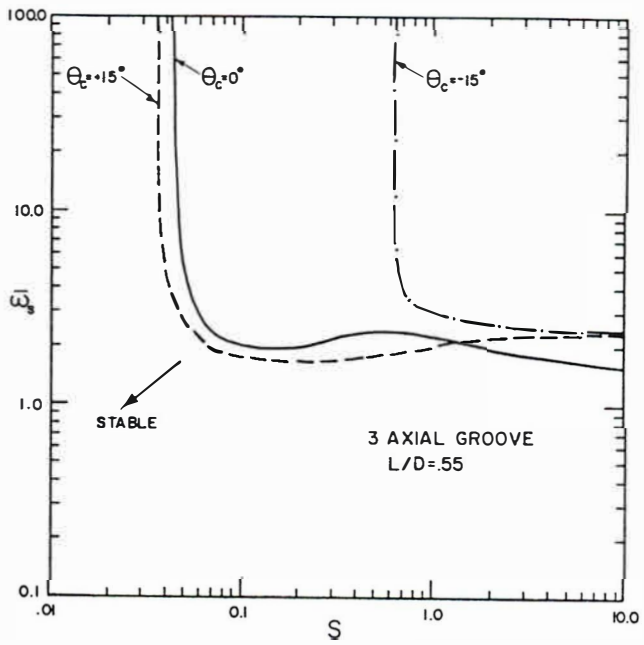

Figure 19 3 Axial Groove Bearing Rigid Rotor Stability

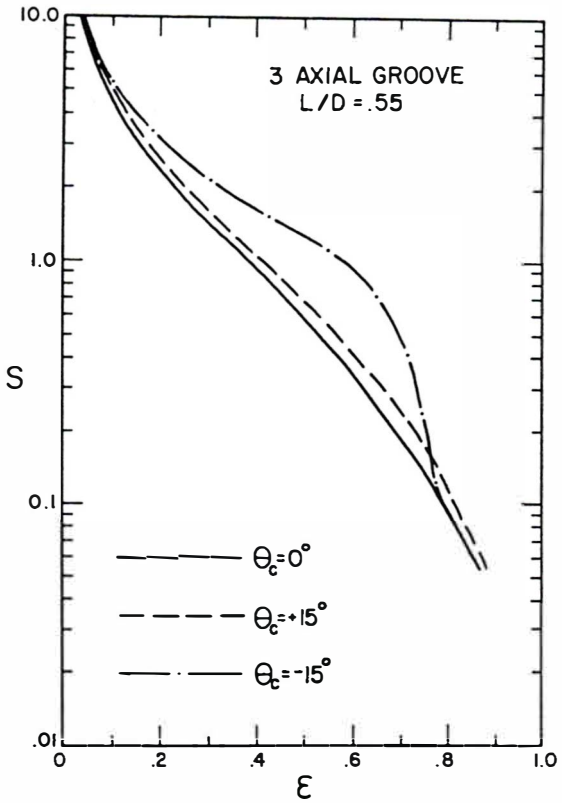

Figure 20 3 Axial Groove Bearing Load Capacity

Double Pocket Bearings (7, 8, 9)

Placing opposed stepped pockets in the upper 2 lobes of a 3 axial groove bearing (Figure 18) produces the bearing stability curves of Figure 21. The 3 axial groove case with $\theta_c = 0°$ is also shown for comparison. Two double pocket clockings are illustrated. The load between oil feed grooves configuration ($\theta_c = 0°$) produces improved stability characteristics in the high Sommerfeld number range (S > 1.0) compared to the 3 axial groove bearing. The double pocket bearing clocked 15° against rotation ($\theta_c = -15°$) provides the same improved stability characteristics in the high Sommerfeld number range plus a much larger region of infinite stability which extends below S = 0.7.

The load curves for the same bearings are illustrated in Figure 22. At high Sommerfeld numbers, the pockets provide an additional hydrodynamic load that forces the journal to operate at a moderate eccentricity ratio even though the external journal loading is light and/or the journal speed is high. The eccentricity approaches $\varepsilon = 0.39$ at S = 10 for both double pocket cases. This additional pocket loading is responsible for the improved stability characteristics in the high Sommerfeld number range.

For the double pocket $\theta_c = -15°$ bearing, infinite stability is achieved below S = 0.7 without a penalty in load capacity. Load curves for the double pocket bearings approach the load curve for the 3 axial groove bearing as S approaches 0.1.

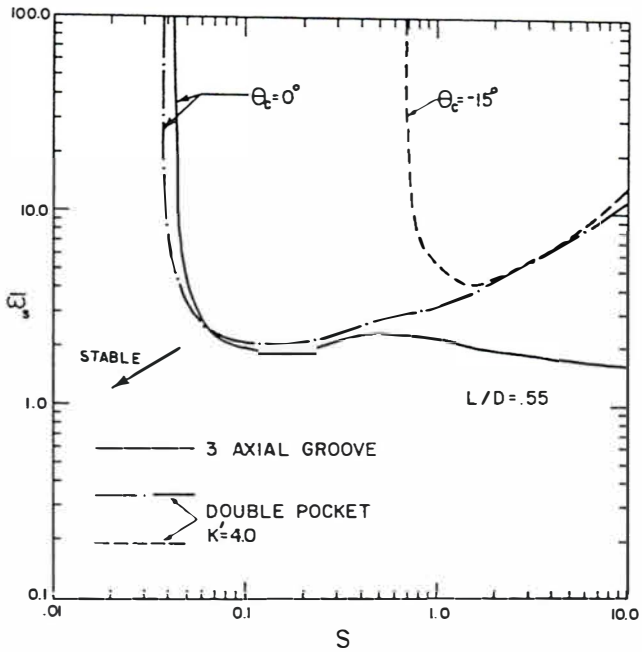

Figure 21 Double Pocket & 3 Axial Groove Bearing Rigid Rotor Stability

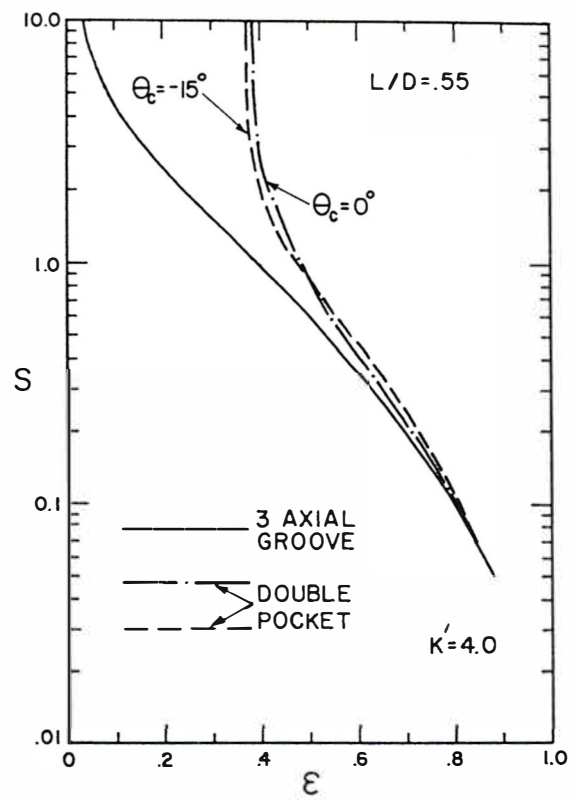

Figure 22 Double Pocket & 3 Axial Groove Bearing Load Capacity

Double Pocket Bearing Gas Turbine Application #1 (9)

A frequency spectrum is shown in Figure 23 for a large overhung power turbine operating on test with 3 axial groove bearings. A large subsynchronous component is evident at 40 Hz (0.033 mm, 1.3 mils at 5,000 rpm) predominately in the horizontal direction. The amplitude of the 40 Hz component exceeded 6.0 mils soon after this signature was recorded. Also indicated on Figure 23 are the synchronous power turbine component labeled "1X" and the synchronous gas generator component labeled "1X GG."

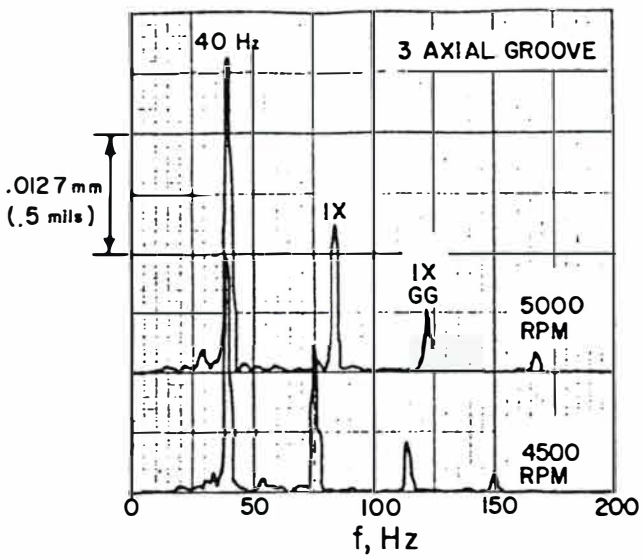

Figure 23 Frequency Spectrum, Power Turbine Test, 3 Axial Groove Bearings

The 40 Hz instability is 48 percent of synchronous speed at 5,000 rpm and is thought to be caused by a combination of oil whirl and aerodynamic excitations from the turbine blades. In an attempt to improve the turbine's stability characteristics, a bearing redesign is considered. The disk end bearing of the power turbine operates at a Sommerfeld number of 0.32. From the bearing stability curves in Figures 19 and 21, the only significant improvement in stability is realized by designing the disk end bearing to operate in the infinite stability region. This may be accomplished by clocking the original 3 axial groove bearing -15° against rotation or clocking the double pocket bearing -15° against rotation.

The clocked 3 axial groove bearing is rejected as a possible bearing modification due to the corresponding loss in capacity as discussed previously. Specifically, the disk end 3 axial groove bearing operates at an eccentricity ratio of 0.62 (S = 0.32, Figure 22). A double pocket modification with θ_c = -15° increases the operating eccentricity to 0.66 while the θ_c = -15°, 3 axial groove design operates at ε = 0.74.

The coupling end bearing operates in the high Sommerfeld number range due to the light bearing load (S = 5.8). The original 3 axial groove bearing with θ_c = 0° is operating on the rigid rotor threshold speed with N_t = 5,043 rpm. Clocking the 3 axial groove bearing -15° increases this speed to 7,416 rpm. However, the double pocket bearing places the stability threshold above 23,000 rpm, well beyond the operating speed of 5,000 rpm.

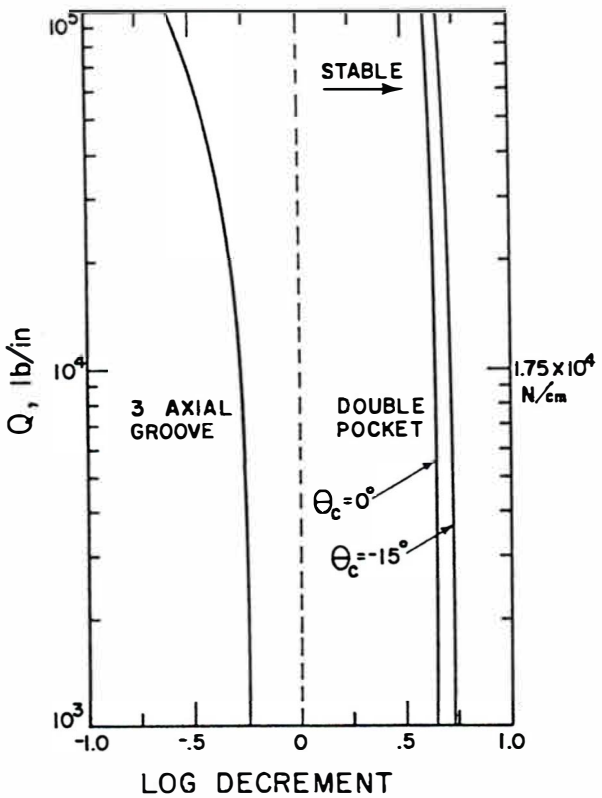

Figure 24 Rotor Bearing System Stability, Power Turbine N = 5,000 rpm

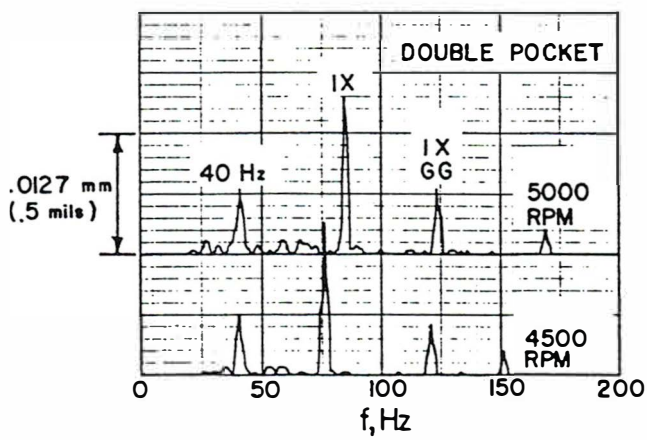

Figure 25 Frequency Spectrum, Power Turbine Test, Double Pocket Bearings

Results from a full rotor-bearing system stability analysis are presented in Figure 24. From Figure 24, logarithmic decrement is plotted against aerodynamic cross-coupling, Q, a destabilizing excitation placed at the turbine disk location. The original design 3 axial groove bearings ($\theta_c = 0°$) place the rotor in the unstable region of the map with a log decrement value of -0.25 for low cross-coupling levels. The damped natural frequency is 2,389 cpm (39.8 Hz) at a cross-coupling level of 1.0×10^4 lb/in. This corresponds to the 40 Hz instability illustrated in Figure 23. Both double pocket bearing designs, however, are well into the stable area with log decrement values above 0.75. The $\theta_c = -15°$ design is slightly more stable than $\theta_c = 0°$ case.

Since the original inserts are clocked 0°, the double pocket $\theta_c = 0°$ design is chosen to replace the 3 axial groove inserts. Figure 25 shows the turbine's frequency spectrum operating on the modified double pocket bearings. The 40 Hz subsynchronous component is suppressed to an amplitude of 0.25 mils at 5,000 rpm. This level is bounded and well within customer specifications.

Double Pocket Bearing Gas Expander Application #2 (4, 7)

A high vibration level in excess of 3.0 mils caused numerous shutdowns of 2 hot gas expanders operating under full load. The rotors were supported on 3 axial groove bearings. Each expander drove a separate multi-stage centrifugal compressor through a gear-type flexible coupling. The two expander-compressor trains are typical of the type of units utilized in the separation process.

Figure 26 shows a sample frequency spectrum, at 5,120 rpm and the large 34 Hz subsynchronous component just prior to trip-out. The 34 Hz vibration grew to around 2.5 mils, and the expander shut down soon after this signature was recorded.

A detailed stability analysis using actual bearing clearances indicated that the rotor-bearing system was unstable as a result of the bearings causing the re-excitation of the expander's first fundamental natural frequency. Utilizing the double pocket design guidelines discussed in the previous section, an optimized step bearing was designed to eliminate the oil-whirl-induced instability. A bearing stability plot is shown in Figure 21

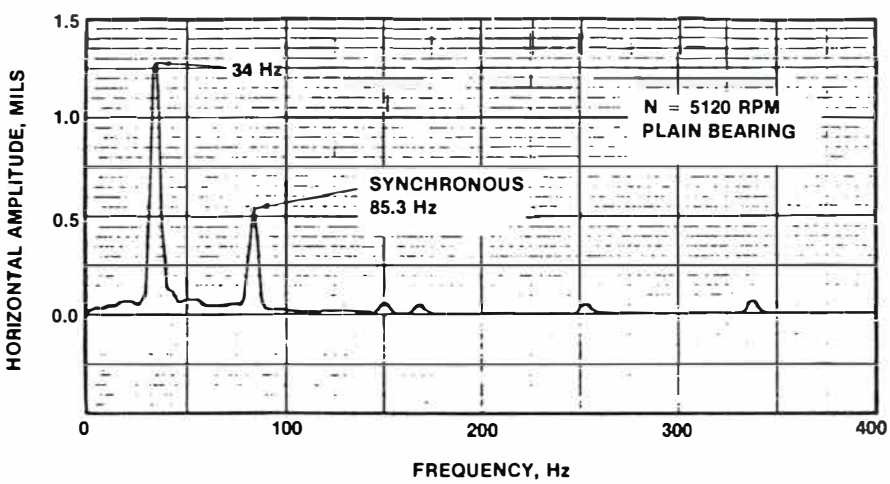

Figure 26 Frequency Spectrum, Hot Gas Expander Test, Original 3 Axial Groove Bearings

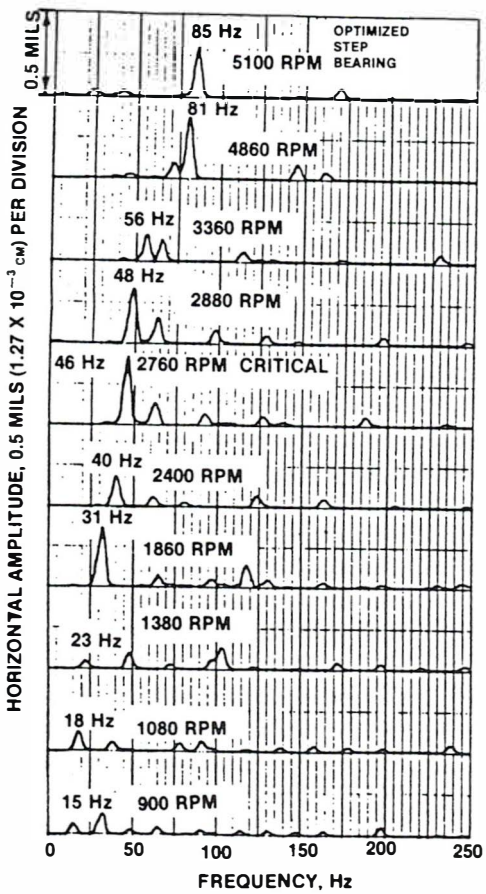

Figure 27 Frequency Spectrum, Hot Gas Expander Test, Double Pocket Bearings

showing the original bearing and the optimized double pocket design. Note the large increase in instability onset speed for the optimized design compared to the plain 3 axial groove bearing.

The 3 axial groove bearings were removed and modified to the optimized double pocket design similar to the design analyzed in Figure 21. The resulting frequency spectrum is shown in Figure 27. The 34 Hz component has been suppressed to an acceptable level that is representative of stable units in service. Both units have operated free of high vibration trip-outs since the bearing redesign was incorporated.

Double Pocket Bearings - Conclusions

A simple, inexpensive and quick modification to stabilize a plain 3 axial groove bearing is to place opposed pockets in the top pads. The pockets increase the stiffness and damping properties (9) and the stability margin compared to the plain bearing while the bottom plain pad retains the load carrying capacity of the original 3 axial groove design. In the high Sommerfeld number range (S > 1.0, high speeds and/or light loads) a substantial increase in stability is realized

with the double pocket bearing. Essentially no additional increase in stability is evident by clocking the double pocket baring 15° against rotation for Sommerfeld numbers greater than 2.0.

Infinite rigid rotor stability is possible in the moderate Sommerfeld number range ($0.1 \leq S \leq 1.0$) by clocking the double pocket bearing 15° against rotation. In this configuration, load capacity does not diminish compared to the un-clocked case or the original 3 axial groove design. This infinite stability condition at moderate Sommerfeld numbers may also be achieved by clocking a 3 axial groove bearing 15° against rotation. However, for this case, the load capacity is greatly diminished.

MULTI-LOBE AND TAPER-LAND BEARINGS (7, 8, 10, 11)

Taper land (Figure 28) and multi-lobe bearings (Figure 29) are also very popular sleeve bearings that are successful in increasing the instability threshold speed compared to cylindrical sleeve bearings. The taper land bearing has side lands similar to a pressure dam and thus is a pocket bearing. Care must be taken when using this design in heavy load applications as load capacity may be a problem (7, 8). Taper land bearings are very frequently utilized in small, light rotors operating at high speeds such as small turbo-expanders, cryogenic expanders and turbochargers.

Multi-lobe bearings (10, 11) do not have side lands. The elliptical bearing is a 2-lobe multi-lobe bearing. The lobes are always preloaded as a zero preloaded multi-lobe bearing is simply an axial groove bearing. The lobes can also be offset with the minimum lobe clearance located at some angle with rotation from the center of the lobe as in Figure 29.

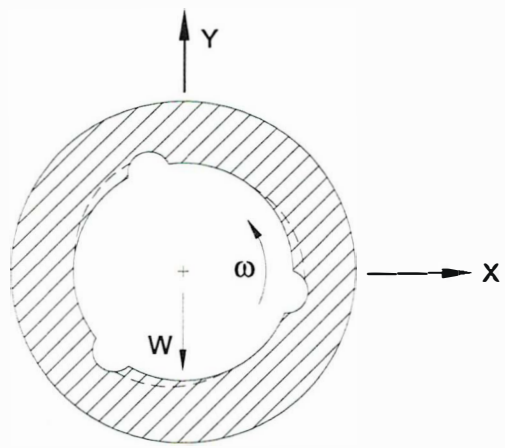

Figure 28 Taper Land Bearing with 3 Tapered Pockets

TILTING PAD BEARINGS (12, 13, 14, 15)

Tilting Pad Bearing Geometric Properties

One advantage of tilting pad bearings is the many design parameters that are available for variation (12, 13, 15). These including pad load orientation, pivot offset, pad preload and pad axial length. First, consider pivot or pad load orientation. The load between pivot configuration is shown in Figure 30. Load between pads provides more symmetric stiffness and damping coefficients (13).

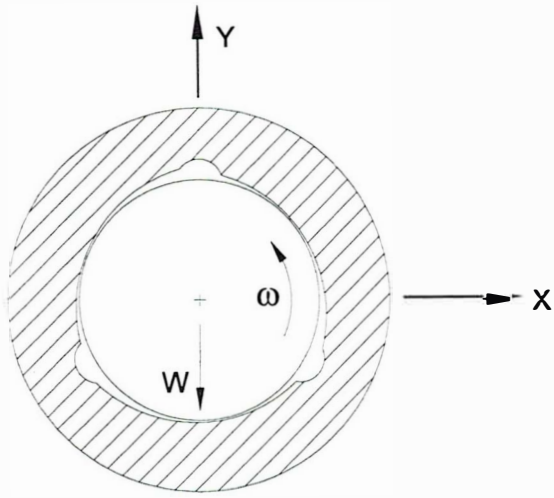

Figure 29 Multi-Lobe Bearing with 3 Preloaded, Offset Lobes

Symmetric support properties provide circular orbits whereas asymmetric supports cause elliptical orbits. Circular orbits are preferable since, in general, their vibration amplitudes are smaller going through a critical compared to the major axis of an elliptical orbit.

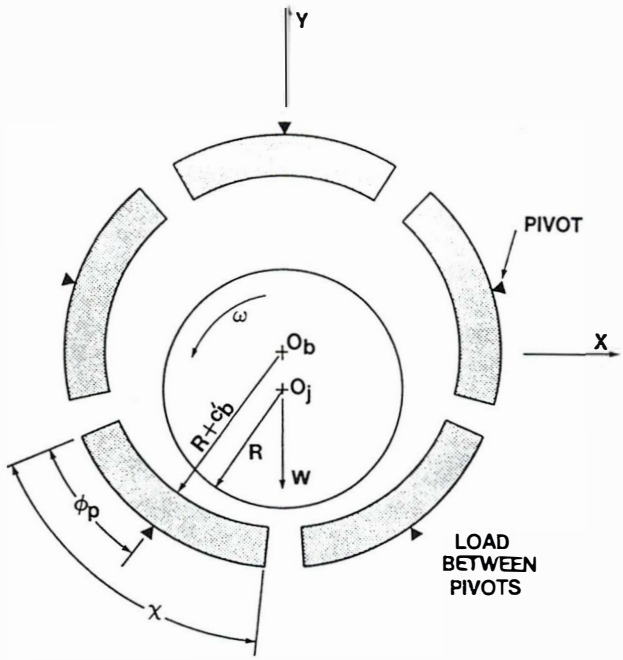

OFFSET, $\alpha = \phi_p / \chi$

Figure 30 Tilting Pad Bearing - Load Between Pivots

Another tilting pad parameter available to the bearing designer is pad pivot offset. Referring to Figure 30, define the pad pivot offset as

$$\alpha = \frac{\phi_p}{\chi} \qquad (17)$$

For centrally pivoted pads, $\alpha = 0.5$ (50% offset). Typical offset pivot values range from $\alpha = 0.55$ to $\alpha = 0.6$ (55 to 60% offset).

Offset pivots are very popular with thrust bearings as offsetting the pivot increases the operating film thickness thereby decreasing the operating temperature (i.e., offset pivots increase bearing load capacity). For tilt pad journal bearings, offset pivots also increase load capacity (12, 15). This translates into lower journal bearing operating temperatures. Also, offset pivots increase bearing stiffness, especially K_{xx}, compared to centrally pivoted pads (12).

Tilting Pad Bearing Preload

Possibly the most important tilting pad bearing parameter available to the bearing designer is tilting pad bearing preload (12- 15). Tilting pad bearing preload is defined as

$$m = 1 - \left(\frac{c_b}{c_p}\right) \qquad (18)$$

For zero preload, the pad machined-in clearance equals the assembled bearing clearance ($c_p = c_b$). When the bearing and journal centers coincide, the journal-to-pad radial clearance at any circumferential location along the pad is constant and equal to the bearing radial clearance, $c'_b = c_b/2$.

For a preloaded pad, the pad clearance is greater than the bearing clearance ($c_p > c_b$). Typical preload values range from 0.0 to 0.5 (0% to 50%). When a pad is preloaded, a converging film section exists even if the journal runs centered in the bearing. Thus, the pad will continue to produce hydrodynamic forces as the bearing load approaches zero.

Tilting Pad Zero Preload Advantages And Disadvantages

The biggest advantage of reducing the tilting pad preload to zero or near zero is illustrated in Figure 31 (13). For this tilt pad bearing example, as preload decreases, bearing damping increases while bearing stiffness remains approximately constant. Both of these trends help in increasing the bearing effective damping. This trend generally holds for a majority of turbomachinery applications.

Effective damping is a measure of how much bearing damping is effective in shaft vibration suppression. As effective damping increases, shaft vibration decreases. Bearing stiffness has a big influence on the amount of effective damping that a bearing produces. Normally, as bearing damping increases, bearing stiffness also increases.

This trend can be seen from Figure 31. As bearing assembled clearance decreases for a constant preload, bearing stiffness and damping both increase. Even though bearing damping increases, the effective damping decreases because the corresponding increase in bearing stiffness makes the bearing damping less effective. The increased bearing stiffness prohibits the shaft from moving in the bearing thereby reducing the effectiveness of the oil film produced damping.

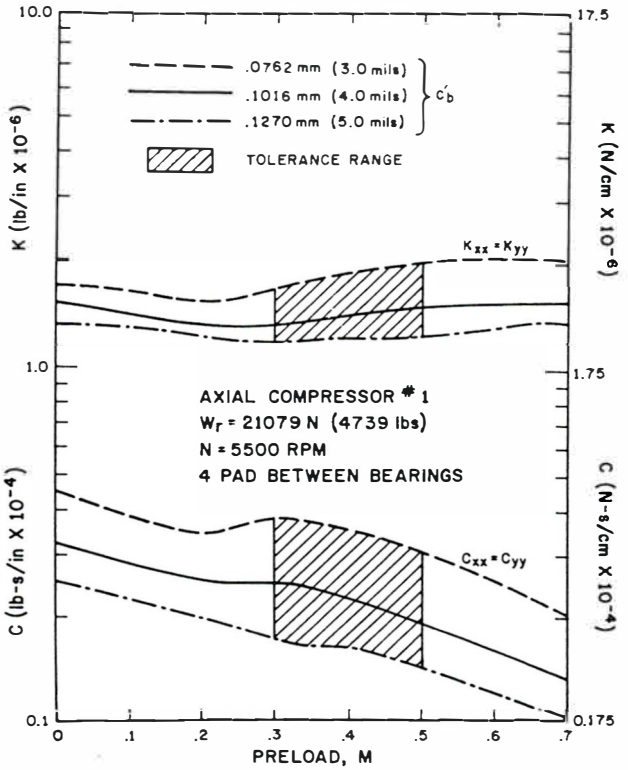

Figure 31 Tilting Pad Bearing Stiffness and Damping vs Preload and Bearing Clearance

Since the decreasing pad preload / increasing effective damping trend is a typical characteristic of many rotor bearing systems, the temptation to decrease tilt pad preload to near zero to improve machine stability is strong. However, there are several major disadvantages to low preload pads. First, there is a drastic decrease in horizontal stiffness and damping (K_{xx} and C_{xx}) as the pad preload becomes negative (15). The problem is the tolerance range. If zero preload is desired, the tolerance range on the journal diameter, the pad radius of curvature and the assembled bearing clearance can all contribute to producing a negative preload.

The second problem with light preload is the loss of damping when the top pads become unloaded. Top unloaded pads also flutter since there does not exist a tilt angle at which the pad can seek equilibrium. Fluttering pads may cause rotor vibration and excessive pivot wear (15).

Tilting Pad L/D Ratio

Another powerful design parameter available to the tilting pad bearing designer is pad length-to-diameter ratio, L/D. An example where increasing the pad L/D ratio *increases* bearing damping but *decreases* bearing stiffness is shown in Figure 32 (13). Again, both changes contribute to the increase in effective damping.

Of course, it is usually more practical to increase the pad length as opposed to decreasing the journal diameter. For this reason,

longer pad lengths have become more popular with bearing designers. The old standard pad L/D = 0.5 is often replaced by L/D = 0.75 or, in extreme cases, with L/D = 1.0.

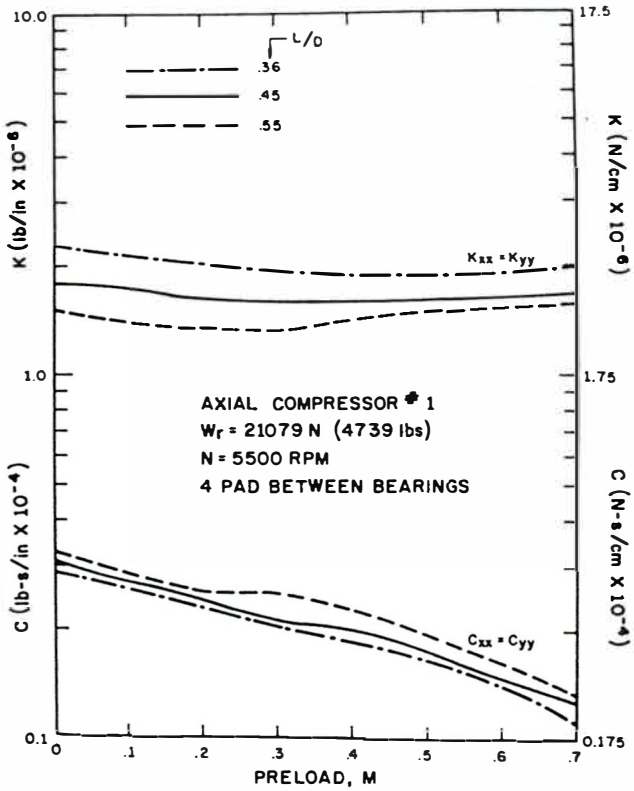

Figure 32 Stiffness and Damping vs Preload and Pad L/D Ratio, 4 Pad Tilting Pad Bearings

BEARING RETROFITS TO SHIFT CRITICAL SPEEDS

Probably the most powerful design tool available to bearing and rotordynamic designers concerns the stiffness and damping asymmetry of sleeve bearings such as axial groove, pressure dam, elliptical or multi-lobe bearings. These asymmetric properties often result in split first critical speeds (13, 14). That is, since the horizontal stiffness and damping are much softer than the vertical, a horizontal first critical speed may appear several hundred to several thousand revolutions per minute lower than the vertical critical.

Tilting pad bearings, however, produce more symmetric bearing properties especially when loaded between pivots. In fact, the stiffness and damping values for a 4 pad tilting pad bearing loaded between pivots are exactly equal (13). This symmetry often results in a single un-split critical that is located approximately midway between the sleeve bearings split peaks (13, 14).

This design tool is illustrated in 3 bearing retrofit case histories presented in the next 3 sections.

Axial Compressor Case History - Sleeve to Tilting Pad Bearing Retrofit to Shift Critical Speeds (13)

This case history considers the design and retrofit application of a 4 pad tilting pad bearing for a relatively heavy (16,210 lb), low speed (3,600 rpm) axial compressor (13). The compressor was originally designed to operate on plain, cylindrical, 3 axial groove sleeve bearings with a unit load of L_u = 179 psi. The actual test stand results for the compressor with 3 axial groove bearings is shown in Figure 33. A peak response is evident at 3,750 rpm which is unacceptably close to the 3,600 rpm operating speed.

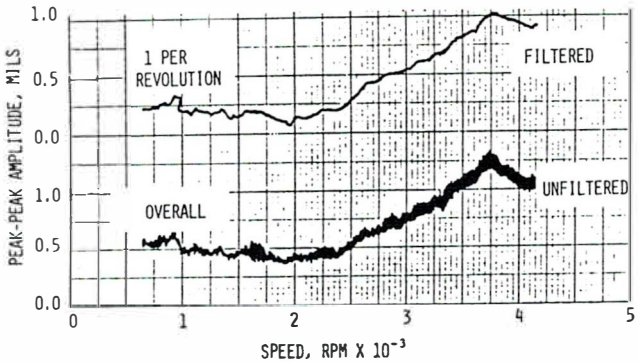

Figure 33 Axial Compressor Actual Test Stand Peak-to-Peak Response, 3 Axial Groove Bearings

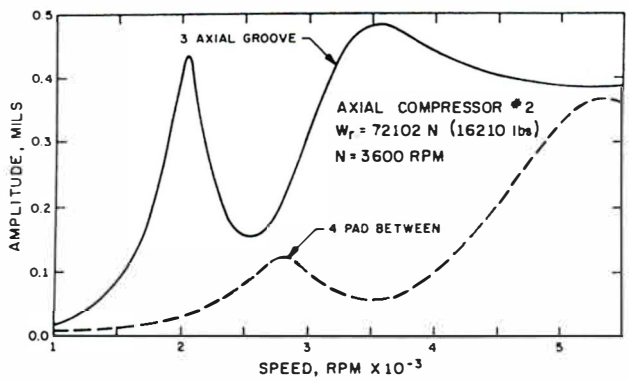

Figure 34 Axial Compressor Analytically Predicted Peak-to-Peak Response

The high unit load on the 3 axial groove bearings produces bearing properties that are extremely asymmetric. This asymmetry results in 2 distinct peaks for the first critical speed. The lower, horizontal peak is non-responsive in Figure 33 and the peak at 3,750 rpm is the higher, vertical first critical. This is illustrated in Figure 34 where an analytical response curve is shown for the axial compressor with the original 3 axial groove bearings. The 3 axial groove predicted response shows 2 peaks at 2,000 and 3,500 rpm. Close examination of the mode shapes and critical speed map indicates that both peaks are first mode criticals due to the asymmetry in the axial groove bearings.

The major advantage of a 4 pad tilting pad bearing is the symmetric stiffness and damping properties that result when loaded between pivots (13). With symmetric dynamic characteristics, the split first mode no longer exists. It is replaced by a single peak located approximately midway between the sleeve bearing split peaks. Figure 34 also shows the predicted response for the axial compressor with a proposed retrofit: a 4 pad tilting pad bearing design with load between pivots. The 4 pad tilting pad bearing with between pivot loading is symmetric and results in only one peak at 2,800 rpm.

Test results for the compressor operating on 4 pad tilting pad bearings with between pivot loading is shown in Figure 35. The critical is now located between 2,850 and 3,000 rpm, 16.7 to 20.8% below operating speed. These results are summarized in Table 2.

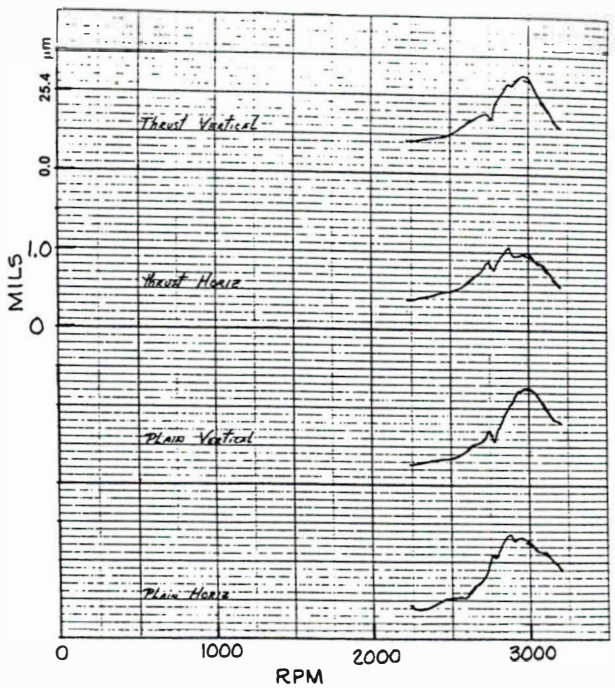

Figure 35 Axial Compressor Actual Test Stand Peak-to-Peak Response, 4 Pad Tilting Pad Bearings

Table 2 Axial Compressor - Comparison of Predicted to Actual Test Stand Results

Parameter	Bearings	Predicted	Actual
Location (rpm)	Original 3AG	3,500	3,750
Amplification	Original 3AG	3.5	5.0
Location (rpm)	Retrofitted 4TP	2,800	2,850-3,000
Amplification	Retrofitted 4TP	4.0	4.0

Induction Motor Case History - Tilting Pad to Sleeve Bearing Retrofit to Shift Critical Speeds (14)

A two pole 5,000 hp induction motor was designed and built as a rigid shaft machine. That is, it was to operate with the first critical speed located at least 20 percent above the synchronous operating speed of 3,600 rpm. Thus, the first critical speed had to be above 4,320 rpm.

The motors relevant mass-elastic rotor dynamic properties include a rotor weight of 4,430 lb, a bearing span of 69.4 in and a journal diameter of 5.5 in.

The resulting test stand response plot is illustrated in Figure 36 for the induction motor operating on the original 4 pad tilting pad bearings. Clearly, the first critical speed, N_1, is located at 3,900 rpm with an associated amplification factor of $A_1 = 5.7$. With 10 oz-in of unbalance placed in-phase at each fan inboard of the bearings, the resulting vibration is 2.5 mils peak-to-peak (pk-pk).

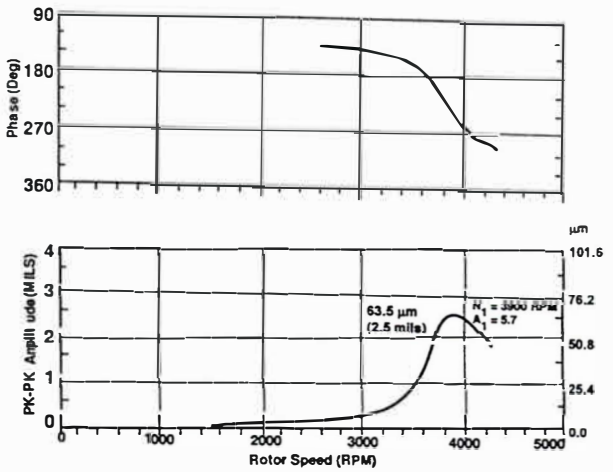

Figure 36 Induction Motor Test Stand Response, Tilting Pad Bearings

The corresponding analytical response plot is shown in Figure 37 with 10 oz-in of unbalance in-phase at each fan. The resulting predicted first critical speed is 3,900 rpm with an amplification factor of 6.4 and 2.6 mils of pk-pk vibration. Unfortunately, the initial analysis assumed an unreasonably high support stiffness (14). Thus, the first critical was initially erroneously predicted above 4,320 rpm.

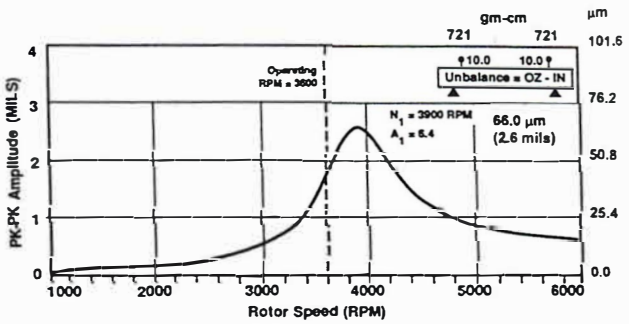

Figure 37 Analytical Response, Induction Motor, Tilting Pad Bearings

Numerous attempts were made to raise the first critical speed by stiffening the bearing support. For example, stiffeners were added to the bearing brackets and the motor was moved around the test floor seeking the least flexible location. However, the first critical speed was still well below the 4,320 rpm separation margin. With two motor rotors already built, the rotor bearing design with the stiffened bearing brackets remained unacceptable to the customer.

After all other design efforts were exhausted short of a complete rotor redesign, an analysis was conducted replacing the original tilting pad bearings with elliptical sleeve bearings. The resulting analytical response plot is shown in Figure 38. Again with 10

oz-in of unbalance at the fan locations, two distinct first criticals are evident. The lower or horizontal first critical, N_h, is located at 2,350 rpm with A_h = 2.2 and with 1.6 mils of pk-pk vibration. The higher, or vertical, first critical, N_v, is at 4,550 rpm with A_v = 3.8. Both criticals now meet the required separation margin.

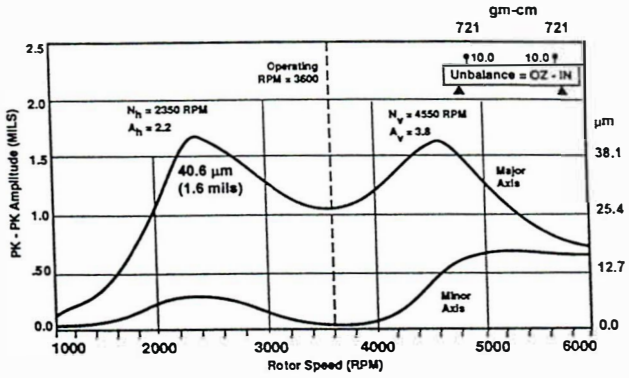

Figure 38 Analytical Response, Induction Motor, Elliptical Sleeve Bearings

The stiffness and damping properties for both tilting pad and elliptical bearings are summarized at 3,600 rpm in Table 3. Note that the 4 pad tilting pad bearing with between pivot loading produces equal horizontal and vertical bearing properties. However, the elliptical bearings vertical stiffness is about 5 times larger than the horizontal stiffness and its vertical damping is a factor of 6.4 times greater than the horizontal. This stiffness and damping asymmetry for the elliptical bearings produces the split first critical speed of Figure 38.

Table 3 Induction Motor - Comparison of 4 Pad Tilting Pad to Elliptical Bearing Dynamic Properties, N = 3,600 rpm

Parameter	4 Pad Tilting Pad	Elliptical
D (mm, in)	139.7 (5.5)	139.7 (5.5)
L (mm, in)	44.45 (1.75)	63.5 (2.5)
W_i (kN, lbf)	9.85 (2,215)	9.85 (2,215)
L_u (MPa, psi)	1.6 (230)	1.1 (161)
K_{xx} (N/cm, lbf/in) x10^{-6}	4.73 (2.70)	1.10 (0.63)
K_{yy} (N/cm, lbf/in) x10^{-6}	4.73 (2.70)	5.46 (3.12)
C_{xx} (N-s/cm, lbf-s/in)	5,516 (3,150)	2,749 (1,570)
C_{yy} (N-s/cm, lbf-s/in)	5,516 (3,150)	17,477 (9,980)

The customer initially objected to losing the tilting pad bearings and rigid shaft design, but soon agreed to attempt the bearing change. It was clear to all concerned that changing to elliptical sleeve bearings was the only viable option.

The resulting test stand plot for the motor with elliptical bearings and with 10 oz-in of in-phase unbalance at the fans is shown in Figure 39. The vibration level is 1.6 mils pk-pk with N_h = 2,740 rpm and A_h = 1.5. Compared to the predicted results, the vibration magnitude and amplification factor are quite close, but the actual location of the critical is 390 rpm higher than predicted. These results are summarized in Table 4.

Note that the higher vertical critical is not evident in Figure 39. The predicted location of N_v is at 4,550 rpm. Since the actual N_h is higher than predicted N_h, the actual N_v should be somewhat higher than 4,550 rpm. Thus, the test stand maximum speed of 4,250 rpm is insufficient to reveal the second peak, N_v, of the predicted split first critical speed.

The customer accepted the induction motors with the elliptical bearings and both units have been operating for about 5 years free of vibration problems.

Table 4 Induction Motor - Comparison of Predicted to Actual Test Stand Results

Parameter	Bearings	Predicted	Actual
Location (rpm)	Original 4TP	3,900	3,900
Amplification	Original 4TP	6.4	5.7
Amplitude (mils)	Original 4TP	2.6	2.5
Location (rpm)	Retrofitted Elliptical	2,350	2,740
Amplification	Retrofitted Elliptical	2.2	1.5
Amplitude (mils)	Retrofitted Elliptical	1.6	1.6

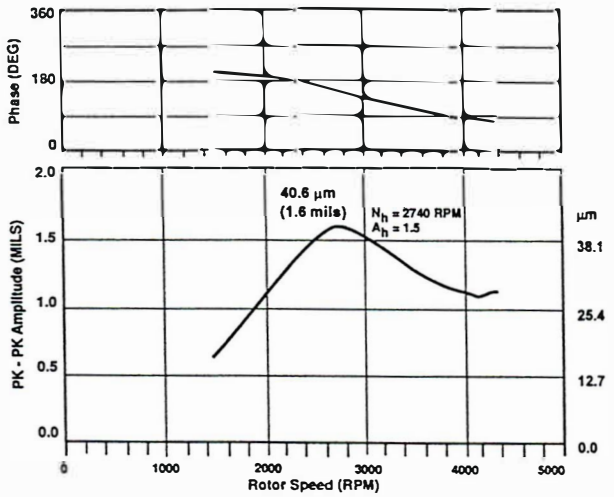

Figure 39 Induction Motor Test Stand Coast Down, Elliptical Sleeve Bearings

Steam Turbine Case History - Tilting Pad to Sleeve Bearing Retrofit to Shift Critical Speeds (14)

A 1940's vintage 12 stage main air blower steam turbine driver in refinery operation underwent a performance and bearing rerate. This type of steam turbine was typically utilized as a blast furnace blower driver. The rerated turbine operated on 5 pad tilting pad bearings. The rerated turbine's bearing span is 105 in with a rotor weight of 12,204 lb and a midshaft diameter of 14.0 in. The turbines speed range is from 2,450 to 2,800 rpm with normal operation at 2,800 rpm. This rerated rotor will be referred to as the original rotor.

The analytically generated response curve for the original rotor with 5 pad tilting pad bearings is illustrated in Figure 40. The first critical speed location is predicted at 2,300 rpm with an

amplification factor of 10.5. Since the minimum speed is 2,450 rpm, the location of the first critical speed is unacceptable. Furthermore, the amplification factor of 10.5 is excessive.

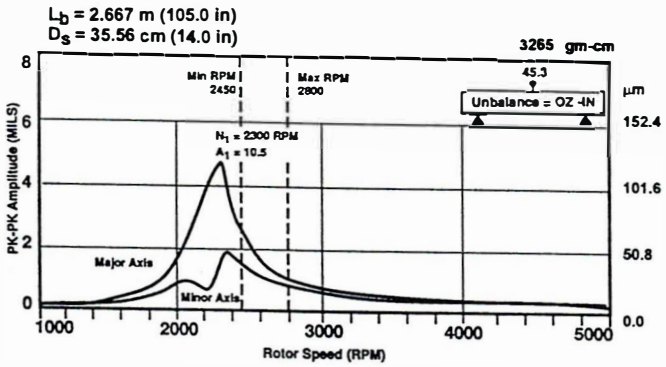

Figure 40 Analytical Response, Steam Turbine Original Rotor, Tilting Pad Bearings

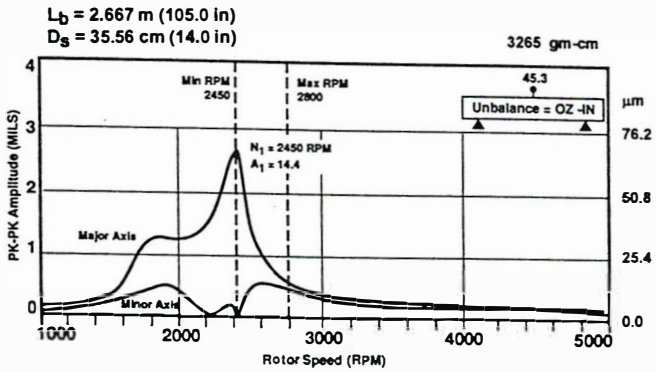

Figure 41 Analytical Response, Steam Turbine Original Rotor, 3 Axial Groove Bearings

Three axial groove bearings were considered in an attempt to split the first critical speed thereby operating between the split peaks. The analytical prediction for the original steam turbine rotor operating on 3 axial groove bearings is shown in Figure 41. Unfortunately, the higher vertical peak shifted by only 150 rpm and is located at the minimum speed of 2,450 with an amplification factor of 14.4. Thus, a sleeve bearing retrofit is unacceptable for this rotor. With the customer unwilling to authorize a rotor change, the 5 pad tilting pad bearings were chosen for the rerated turbine.

Actual field results from a coupled run for the original rotor with 5 pad tilting pad bearings are shown in Figure 42. The first critical appears to be located between 2,600 and 2,750 rpm with A_1 = 11.0 and vibration levels at 7.0 mils pk-pk. The turbine operated continuously for over 3 years in this condition with vibration readings that were typically in the 7.0 mils pk-pk range.

Due to the resulting high vibration levels and close proximity of the actual critical speed to the maximum operating speed, a rotor redesign was undertaken. It was convenient to increase the midshaft diameter from 14.0 in to 16.5 in and to decrease the bearing span from 105 to 100 in.

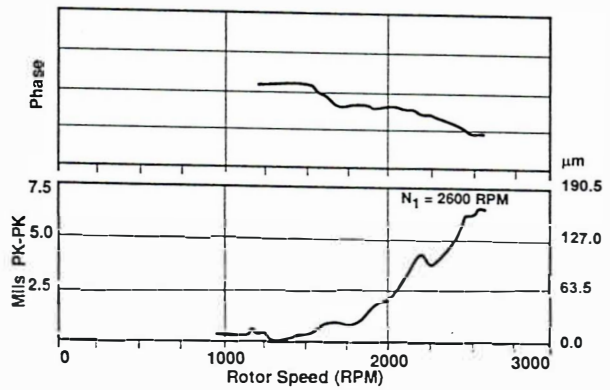

Figure 42 Steam Turbine Field Coast Down, Original Rotor, Tilting Pad Bearings

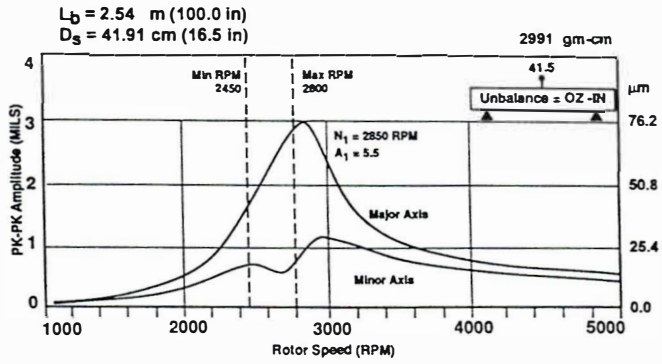

Figure 43 Analytical Response, Steam Turbine Redesigned Rotor, Tilting Pad Bearings

The resulting speed-amplitude plot with tilting pad bearings is illustrated in Figure 43. While the amplification factor decreased considerably from 10.5 (Figure 40) to 5.5, the predicted location of the first critical speed is 2,850 rpm, which is unacceptably close to the maximum operating speed of 2,800 rpm.

Again, 3 axial groove bearings were considered in an attempt to split the first critical speed thereby operating between the split peaks. A response plot for the redesigned rotor with 3 axial groove sleeve bearings is presented in Figure 44. Now the first critical speed is split with the lower horizontal critical located at 2,150 rpm, A_h = 3.6 and higher vertical critical at 3,150 rpm, A_v = 7.9. The turbine's operating speed range of 2,450 to 2,800 rpm is between the 2 first critical peaks.

A summary of bearing characteristics for the tilting pad and the 3 axial groove bearings is shown in Table 5. Even though the principle stiffness asymmetry for the axial groove bearings is not as great compared to the tilting pad bearing, the damping asymmetry increases from about a factor of 2 for the tilting pad design to a factor of 4 for the axial groove design. This damping asymmetry results in the split first critical peaks presented in Figure 44.

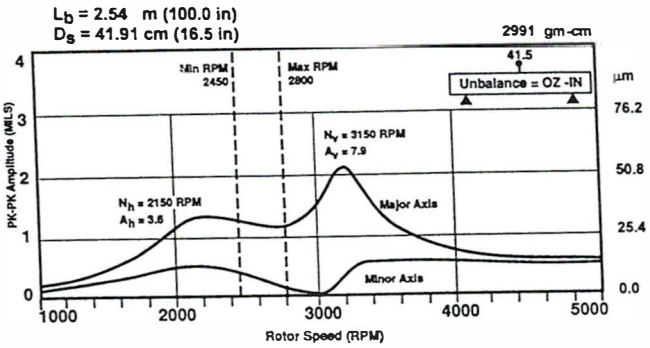

Figure 44 Analytical Response, Steam Turbine Redesigned Rotor, 3 Axial Groove Bearings

Table 5 Steam Turbine - Comparison of Tilting Pad to 3 Axial Groove Bearing Stiffness and Damping Properties at N = 2,800 rpm

Parameter	5 Pad Tilting Pad	3 Axial Groove
D (mm, in)	177.8 (7.0)	177.8 (7.0)
L (mm, in)	133.4 (5.25)	177.8 (7.0)
W_t (kN, lbf)	25.73 (5,785)	25.73 (5,785)
L_u (MPa, psi)	1.1 (157)	0.8 (118)
K_{xx} (N/cm, lbf/in) x10^{-6}	4.33 (2.47)	4.22 (2.41)
K_{yy} (N/cm, lbf/in) x10^{-6}	8.14 (4.65)	5.59 (3.19)
C_{xx} (N-s/cm, lbf-s/in)	8,266 (4,720)	16,934 (9,670)
C_{yy} (N-s/cm, lbf-s/in)	14,727 (8,410)	67,946 (38,800)

The redesigned rotor was manufactured with the intent to use the 3 axial groove bearings. The customer requested a high speed balance for a balance check and verification of the locations of the critical speed peaks. Problems locating the bearings correctly in high speed balance facility caused the bearing span to temporarily increase from 100.0 to 103.0 in.

Actual coast down response plots from the high speed balance facility are shown in Figure 45. The predicted first critical split peak is not evident as the lower horizontal first critical is indeed critically damped and cannot be seen in Figure 45. The higher vertical first critical is located at 3,000 rpm with A_v = 4.1. These results are summarized in Table 6.

Table 6 Steam Turbine - Comparison of Predicted to Actual High Speed Balance and Field Results

Parameter	Bearings	Predicted	Actual
Location (rpm)	Original 5TP	2,300	2,600-2,750
Amplification	Original 5TP	10.5	11.0
Location (rpm)	Retrofitted 3AG	3,150	3,000
Amplification	Retrofitted 3AG	7.9	4.1

Uncoupled, on-site response tests for the redesigned rotor with 3 axial groove bearings show no indication of critical peaks anywhere up to the trip speed of 3,080 rpm confirming a non-responsive horizontal first critical and a vertical first critical above 3,080 rpm (14). The turbine has been operating for over 4 years under 0.5 mils of pk-pk vibration at an increased maximum continuous speed of 2,900 rpm.

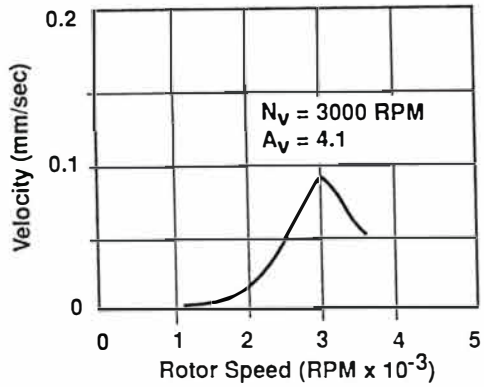

Figure 45 Steam Turbine High Speed Balance, Redesigned Rotor, 3 Axial Groove Bearings

Discussion - Tilting Pad to Sleeve Bearing Retrofit to Shift Critical Speeds (14)

Retrofitting or changing from tilting pad to sleeve bearings to split the first critical speed should be attempted only if the current rotor bearing system meets several criteria. One of these design rules is that the operating speed should be below 5,000 rpm to prevent oil whirl problems with the sleeve bearings. A second rule is that the sleeve bearing unit loading, L_u, should be above 100 psi to insure a sufficient separation between the first critical speed peaks. Both cases presented here meet these criteria. The induction motor runs at 3,600 rpm with an elliptical bearing unit load of 161 psi. The steam turbine operates below 2,900 rpm with a 3 axial groove bearing unit load of 118 psi.

Another important criterion concerns amplification factor. As the amplification factor increases, the ratio of shaft stiffness to bearing stiffness decreases, thereby reducing the ability of the bearing stiffness and damping properties to affect the rotor bearing system. That is, both the bearing stiffness and damping properties become less and less effective in locating the rotor's critical speeds. Thus, a tilting pad to sleeve bearing retrofit to split a critical speed should not be contemplated for tilting pad system criticals whose amplification factors are greater that 8.0. As the amplification factor increases, the split between the horizontal and vertical critical peaks decreases.

For the 2 cases discussed here, the induction motor's first critical amplification factor with tilting pad bearings is 5.7 from Figure 36 (actual test stand response curve) and 6.4 from Figure 37 (analytical response curve) . The steam turbine's first critical amplification factor of the redesigned rotor with tilting pad bearings is 5.5 from the analytical response plot in Figure 43.

Note that the original steam turbine rotor with tilting pad bearings has a first critical amplification factor of 10.5 (Figure 40). An attempt to split this critical with a sleeve bearing was unsuccessful due to the high amplification factor (Figure 41). Therefore, a 2 step approach was necessary. First, the shaft stiffness was increased by increasing the midshaft diameter and decreasing the bearing span, thereby reducing the amplification factor with tilting pad bearings to 5.5 (Figure 43). Then, with a much lower amplification factor, the journal bearings were switched from tilting pad to 3 axial groove and the first critical peak was successfully split (Figure 44).

NOMENCLATURE

A_1, A_h, A_v	first critical, horizontal critical, vertical critical amplification factor (dim)
c, c_1, c_2	sleeve bearing radial clearance (mm, in)
c_b, c'_b	tilting pad bearing diametral, radial clearance (mm, in)
c_d	pocket radial clearance (mm,in)
c_p, c'_p	tilting pad diametral, radial clearance (mm, in)
C, C_{ij}	bearing damping (N-s/cm, lbf-s/in)
C_{xx}, C_{yy}	bearing damping in the horizontal, vertical direction (N-s/cm, lbf-s/in)
$\bar{C}_{xx}$, $\bar{C}_{yy}$	dimensionless bearing damping in the horizontal, vertical direction (dim)
d	offset from bearing center (mm, in)
D, D_s	journal, mid-shaft diameter (mm, in)
e	bearing eccentricity (mm, in)
g	acceleration of gravity (m/s^2, in/s^2)
h_s, h_{min}	pocket depth, minimum film thickness (mm, in)
K', K_1', K_2'	= c_d/c = pocket clearance ratio (dim)
K, K_{ij}	bearing stiffness (N/cm, lbf/in)
K_{xx}, K_{yy}	bearing stiffness in the horizontal, vertical direction (N/cm, lbf/in)
$\bar{K}_{xx}$, $\bar{K}_{xx}$	dimensionless bearing stiffness in the horizontal, vertical direction (dim)
L, L_b	bearing axial length, bearing span (mm, in)
L_u	= (LxD)/W = bearing unit load (MPa, psi)
L_d, L_t	pocket, relief track axial length (mm, in)
$\bar{L}_d$, $\bar{L}_t$	pocket, relief track axial length ratio (dim)
m'	journal mass (slug = $lbf\text{-}s^2/f$)
M'	= $m'c\omega_s^2/W$
m, M	tilt pad bearing preload (dim)
N, N_s	journal rotational speed (rpm, rps)
N_1, N_h, N_v	first, horizontal, vertical critical speed (rpm)
N_t	instability threshold speed, (rpm)
O_b, O_j	bearing, pad, journal center (dim)
Q	aerodynamic cross-coupling (N/cm, lbf/in)
R', R_x, R_y	external non-gravity load (N,lbf)
R	journal radius (mm, in)
R_e	Reynolds number (dim)
S	Sommerfeld number (dim)
W, W_j	journal total load, gravity load (N, lbf)
W_t, W_r	total rotor weight (N, lbf)
W_g	resultant gear force (N, lbf)
α	tilt pad pivot offset (dim)
ε	bearing eccentricity ratio (dim)
θ_c	sleeve bearing clocking angle (deg)
θ_r	angle to resultant load vector (deg)
θ_s	pressure dam step location (deg)
μ	oil viscosity (Pa-s, $lbf\text{-}s/in^2$)
ϕ_p	tilt pad pivot angle (deg)
χ	pad arc length (deg)
Ψ	bearing attitude angle (deg)
ω, ω_j	journal rotational speed (1/s)
ω_{cr}	rotor rigid support critical speed (1/s)
ω_s, $\bar{\omega}_s$, $\bar{\omega}$	rigid rotor threshold speed (1/s, dim, dim)
$\bar{\omega}_{sf}$	flexible rotor threshold speed (dim)

REFERENCES

1. Nicholas, J. C., Allaire, P. E., "Analysis of Step Journal Bearings - Finite Length, Stability," ASLE Transactions, 23 (2), pp. 197-207 (April 1980).

2. Nicholas, J. C., Barrett, L. E., Leader, M. E., "Experimental-Theoretical Comparison of Instability Onset Speeds for a Three Mass Rotor Supported by Step Journal Bearings," ASME Journal of Mechanical Design, 102, (2), pp. 344-351 (April 1980).

3. Nicholas, J. C., Allaire, P. E., Lewis, D. W., "Stiffness and Damping Coefficients for Finite Length Step Journal Bearings," ASLE Transactions, 23 (4), pp. 353-362 (October 1980).

4. Nicholas, J. C., "Stabilizing Turbomachinery with Pressure Dam Bearings," *Encyclopedia of Fluid Mechanics*, 2, Gulf Publishing Co. (1986).

5. Mehta, N. P., Singh, A., Gupta, B. K., "Stability of Finite Elliptical Pressure Dam Bearings with Rotor Flexibility Effects", ASLE Transactions, 24 (2), pp. 269-275 (April 1981).

6. Mehta, N. P., Singh, A., "Stability Analysis of Finite Offset-Halves Pressure Dam Bearings", ASME Journal of Tribology, 108 (2), pp. 270-274 (April 1986).

7. Nicholas, J. C., Kirk R. G., "Theory and Application of Multi-Pocket Bearings for Optimum Turborotor Stability," ASLE Transactions, 24 (2), pp. 269-275 (April 1981).

8. Nicholas, J. C., "Double Pocket Bearing Design and Application," *Computer-Aided Lubrication Analysis and Bearing Design*, an ASME publication (October 1982).

9. Nicholas, J. C., "Stability, Load Capacity, Stiffness and Damping Advantages of the Double Pocket Journal Bearing," ASME Journal of Tribology, 107 (1), pp. 53-58 (January 1985).

10. Flack, R. D., Lanes, R. F., "Effects of Three-Lobe Bearing Geometries on Rigid-Rotor Stability", ASLE Transactions, 25 (2), pp. 221-228 (April 1982).

11. Lanes, R. F., Flack, R. D., "Effects of Three-Lobe Bearing Geometries on Flexible Rotor Stability", ASLE Transactions, 25 (3), pp. 377-385 (July 1982).

12. Nicholas, J. C., Gunter, E. J., Allaire, P. E., "Stiffness and Damping Coefficients for the Five Pad Tilting Pad Bearing," ASLE Transactions, *22* (2), pp. 112-124 (April 1979).

13. Nicholas, J. C., Kirk R. G., "Four Pad Tilting Pad Bearing Design and Application for Multi-Stage Axial Compressors," ASME Journal of Lubrication Technology, *104* (4), pp. 523-532 (October 1982).

14. Nicholas, J. C., Moll, R. W., "Shifting Critical Speeds Out of the Operating Range by Changing from Tilting Pad to Sleeve Bearings," *Proceedings of the Twenty-Second Turbomachinery Symposium*, The Turbomachinery Laboratory, Texas A&M University, College Station, Texas (1993).

15. Nicholas, J. C., "Tilting Pad Bearing Design," *Proceedings of the Twenty-Third Turbomachinery Symposium*, The Turbomachinery Laboratory, Texas A&M University, College Station, Texas (1994).

Originally Published in *Mini Course Notes*
Vibration Institute
Willowbrook, Illinois
20th Annual Meeting
St. Louis, Missouri
June 25-27, 1996

Rotating Machinery Technology, Inc.
4181 Bolivar Road
Wellsville, NY 14895
716-593-3700
716-593-2693 (fax)